

1 **Changes in temperature and oxygen isotopic composition of Mediterranean water**
2 **during the Mid-Pleistocene transition in the Montalbano Jonico section (southern**
3 **Italy) using the clumped-isotope thermometer.**

4
5 Marion Peral^{*1,2}, Dominique Blamart¹, Franck Bassinot¹, Mathieu Daëron¹, Fabien
6 Dewilde^{1,3}, Helene Rebaubier¹, Sebastien Nomade¹, Angela Girone⁴, Maria Marino⁴,
7 Patrizia Maiorano⁴, Neri Ciaranfi⁴

8
9 *1. Laboratoire des Sciences du Climat et de l'Environnement, UMR8212, LSCE/IPSL, CEA-CNRS-*
10 *UVSQ and University of Paris-Saclay, Gif-sur-Yvette, France*

11 *2. Now. School of Earth Science, University of Melbourne, 253-283 Elgin St, Carlton, VIC 3053,*
12 *Australia*

13 *3. Institut Universitaire Européen de la Mer, Université de Bretagne Occidentale, CNRS UMS3113,*
14 *Place Nicolas Copernic, 29280 Plouzané*

15 *4. Dipartimento di Scienze della Terra e Geoambientali, Università degli Studi di Bari Aldo Moro,*
16 *via E. Orabona 4, 70125 Bari, Italy*

17
18 * Email of corresponding author: marion.peral@unimelb.edu.au

19
20 **Abstract**

21
22 Taking advantage of the recent clumped-isotope methodological developments, the
23 present study focuses on the reconstruction of temperatures and seawater $\delta^{18}\text{O}$ in the
24 central Mediterranean Sea across the Mid-Pleistocene section from Montalbano Jonico
25 (south of Italy). Our results suggest that Mg/Ca paleothermometer can be biased over
26 several intervals, making clumped-isotope a promising choice to reconstruct past
27 changes in seawater temperature and isotopic composition in the Mediterranean Sea.
28 Our results provide the first clumped-isotope temperature and $\delta^{18}\text{O}_{\text{sw}}$ reconstruction
29 across several glacial and interglacial Marine Isotope Stages from MIS 36 to MIS 19 in
30 the central Mediterranean Sea.

31 During the climatic optimums of MIS 31 and MIS 19, considered as close analogues to
32 the current interglacial in terms of insolation forcing, reconstructed average sub-surface
33 temperatures from benthic foraminifer analyses ($13.8 \pm 1.5^\circ\text{C}$ and $14.8 \pm 1.3^\circ\text{C}$,
34 respectively) and isotopic composition of seawater (between 1.6 ± 0.4 ‰ and 2.0 ± 0.3
35 ‰) are similar to the ones measured today below the thermocline in the Gulf of
36 Taranto. Our results show that bottom water conditions remained similar in all the
37 studied glacial periods, with cold temperatures around $\sim 8^\circ\text{C}$ in average. The lack of a
38 clear cooling across the Mid-Pleistocene either suggest that glacial oceanographic
39 conditions in the Mediterranean Sea remained relatively stable between the 41 ka-world

40 and the 100 ka-world or that the tectonic uplift that took place during this transition
41 balanced out the MPT cooling trend through the shallowing of the deposition site.

42

43 **Keywords:** Paleoceanography, MIS 19, MIS 31, paleothermometry, Mg/Ca, foraminifera,
44 stable isotope

45

46 **1. Introduction**

47

48 The Early- Mid-Pleistocene is a particularly puzzling time interval characterized
49 by a major change in the frequency and amplitude of glacial-interglacial cycles, with a
50 shift from low amplitude, obliquity-dominated climate changes (41 ka cycles) to larger
51 amplitude ~ 100 -ka dominated cycles (Ruddiman et al., 1986; Lisiecki and Raymo, 2005;
52 Lang and Wolff, 2011; Head and Gibbard, 2015). This transition (Mid-Pleistocene
53 Transition, noted MPT) corresponds to an intensification of glacial periods and an
54 increase of their duration (Lisiecki and Raymo, 2005; Head and Gibbard, 2015 and
55 references therein), with Marine Isotopic Stage (MIS) 22 being sometime considered as
56 the precursor of glacial periods typical of the 100 ka-world. Paleo-temperature
57 reconstructions are particularly important to better understand the Mid-Pleistocene
58 evolution and try to disentangle the temperature from the ice volume effect in
59 foraminifer $\delta^{18}\text{O}$ records. However, long time marine paleo-temperature reconstructions
60 are rare across this period and several problems have been raised regarding usual
61 paleo-thermometers. This is the case, in particular, for potential salinity and pH biases
62 on the Mg/Ca paleo-thermometer (Mathien-Blard and Bassinot, 2009; Gray et al., 2018
63 and references therein), which cannot be dealt with easily for the MPT.

64 In the present study, we take advantage of the recently developed clumped
65 isotope thermometry to reconstruct sea-water temperature and $\delta^{18}\text{O}$ changes across the
66 MPT in the context of the Mediterranean Sea using the exposed Montalbano Jonico
67 section (south Italy, Gulf of Taranto, central Mediterranean; Figure 1). The carbonate
68 clumped-isotope thermometer, noted Δ_{47} is based on the quantification of subtle
69 statistical anomalies in the abundance of the doubly substituted carbonate isotopologue
70 ($^{13}\text{C}^{18}\text{O}^{16}\text{O}^{16}\text{O}$) compared to a stochastic distribution of isotopes (Ghosh et al., 2006;
71 Eiler, 2007, Eiler, 2011). For thermodynamical reasons, Δ_{47} varies with temperature
72 (Schauble et al., 2006). As a result, the slightly higher abundance of ^{13}C - ^{18}O bonds

73 decreases systematically with mineral crystallisation temperature. The main advantages
74 of the Δ_{47} thermometer compared to other more frequently used geochemical
75 paleotemperature proxies (such as $\delta^{18}\text{O}$ and Mg/Ca) are the absence of detectable
76 species-specific and salinity effects in both planktonic and benthic foraminifera (Tripathi
77 et al., 2010; Grauel et al., 2013; Peral et al., 2018) and the fact that it does not require
78 any knowledge of seawater $\delta^{18}\text{O}$ (noted $\delta^{18}\text{O}_{\text{sw}}$ hereafter) in which the carbonate
79 calcified (Schauble et al., 2006). Thus, combining Δ_{47} and $\delta^{18}\text{O}_{\text{c}}$ measurements in
80 foraminifera allows reconstructing both past seawater temperatures and $\delta^{18}\text{O}_{\text{sw}}$.

81 We decided to focus our study on the exposed Montalbano Jonico section (MJS,
82 south Italy, Gulf of Taranto, central Mediterranean; Figure 1), which is one of the
83 highest-resolution marine sedimentary record spanning the MPT (Bertini et al., 2015;
84 Marino et al., 2015). Being a semi-enclosed basin, the Mediterranean Sea can amplify
85 climate changes and its geographic position makes it sensitive to both tropical and high-
86 latitude influences (Hurrell, 1995; Trigo et al., 2004; Giorgi, 2006; Lionello et al., 2006).
87 Several studies have already revealed the clear imprint of MPT changes on the
88 Mediterranean marine and continental environments (Johanin et al., 2008; Pol et al.,
89 2010; Giaccio et al., 2015; Wagner et al., 2019). In the MJS, the benthic and planktonic
90 $\delta^{18}\text{O}$ records show the clear alternation between glacial and interglacial periods, and a
91 small enrichment of glacial benthic $\delta^{18}\text{O}$ across the MPT (Figure 2; Brilli, 1998). There
92 exists no accurately quantified-marine temperature and $\delta^{18}\text{O}_{\text{sw}}$ records over this key
93 time interval yet. The exposed Montalbano Jonico section allows to collect large amounts
94 of sedimentary material, which are necessary to replicate clumped-isotope analyses in
95 order to reduce analytical uncertainties and provide the most accurate reconstruction
96 possible of Δ_{47} -temperature changes along the Mid-Pleistocene of the central
97 Mediterranean Sea.

98

99 **2. Strategy and main objectives**

100

101 When dealing with the Mid-Pleistocene interval, two periods are of particular
102 interest: marine isotopic stages (MIS) 31 and 19. The MIS 31, also called “super
103 interglacial” (Pollard and DeConto, 2009; DeConto et al., 2012; Melles et al., 2014; Coletti
104 et al., 2015), extends from about 1.082 to 1.062 Ma (Lisiecki and Raymo, 2005). It is an
105 unusually long interglacial for the 41 ka-world and numerous authors suggested that it

106 could be a precursor of the high-amplitude ~ 100 ka cycles (e.g. Scherer et al., 2008;
107 Girone et al., 2013). This interglacial is characterized by the highest summer insolation
108 forcing of the Pleistocene (Laskar et al., 2004), while indirect pCO₂ reconstructions
109 suggest concentration around 300 ppm at 1.0 Ma (Hönisch et al., 2009). In high latitudes
110 and particularly in the North Atlantic, most of MIS 31 records point toward warm
111 oceanic temperatures (Helmke et al., 2003; Bintanja et al., 2005; Bintanja and Van de
112 Wal, 2008; Naafs et al., 2013), with differences, however, in the magnitude of this
113 warming (Ruddiman et al., 1989; McClymont et al., 2008; Hillaire-Marcel et al., 2011;
114 Oliveira et al., 2017). Several studies have focused on MIS 19 (Pol et al., 2010; Tzedakis
115 et al. 2012; Giaccio et al., 2015; Maiorano et al., 2016; Nomade et al., 2019; Regattieri et
116 al., 2019). They documented changes in the terrestrial and marine realms with
117 continuous and high-resolution records and especially for the interglacial *sensu-stricto*
118 (i.e. MIS 19c hereafter; Tzedakis et al., 2012; Giaccio et al., 2015; Sánchez-Goñi et al.,
119 2016; Nomade et al., 2019). These records depict a shorter climatic optimum compared
120 to MIS 31 (i.e. 10 ka up to 13 ka) followed by millennial- to-centennial-scale climate
121 oscillations, particularly well-expressed within the substages 19a and 19b (Tzedakis et
122 al., 2012; Giaccio et al., 2015; Sánchez-Goñi et al., 2016; Regattieri et al., 2018; Nomade
123 et al., 2019).

124 The onset of these two interglacials are characterized by insolation forcing
125 conditions that are relatively similar to those that prevailed during the onset of the
126 Holocene (high obliquity, low precession), making these two MIS good candidates to
127 study the response of the Mediterranean Sea under an orbital forcing similar to the
128 Holocene but, presumably, under different mean climate conditions and greenhouse gas
129 composition of the atmosphere.

130

131 The MJS is divided into two parts: Interval A (lower part of the section – 168 m
132 thick, from MIS 37 to MIS 23) and Interval B (upper part of the section – 280 m thick;
133 from MIS22 to the MIS17/16 transition), separated by a stratigraphic gap estimated to
134 last about 19 ka (Ciaranfi et al., 2010; Figure 2). As already mentioned above, available
135 $\delta^{18}\text{O}$ data suggest a slight increase in glacial benthic $\delta^{18}\text{O}$ values between section A and
136 section B, accompanied by an increase in the difference between planktonic and benthic
137 $\delta^{18}\text{O}$ values. Such evolution does seem to be coherent with an intensification of glacials
138 across the MPT. However, paleo-water depth reconstruction based on benthic

139 foraminifer assemblages suggests that the depth of deposition of MJS varied from a
140 bathyal environment in the Interval A to a circalittoral environment in the Interval B
141 (Stefanelli, 2003). The transition from a deeper to a shallower environment appears
142 relatively abrupt and synchronous to the stratigraphic gap observed between Intervals
143 A and B, corresponding to the transition between MIS 23 – MIS 22 (Figure 2; Stefanelli,
144 2003). This shallowing has been attributed to a tectonic uplifting. The evolution of
145 vertical $\delta^{18}\text{O}$ gradients (i.e. planktonic-benthic difference) and the slight increase in
146 glacial benthic $\delta^{18}\text{O}$ across the MPT are counter-intuitive when considering that they
147 took place during an important shallowing of the deposition site. In order to better
148 constrain the relative importance of oceanographic and tectonic imprints in the Mid-
149 Pleistocene evolution of glacial conditions recorded in MJS, we propose to separate
150 temperature and $\delta^{18}\text{O}_{\text{sw}}$ effects in the benthic $\delta^{18}\text{O}$ record and compare the evolution of
151 glacial periods from interval A (MIS 36, MIS 34 and MIS 30) with those from interval B
152 (MIS 22 and MIS 20).

153 The present paper aims at two main objectives: 1) comparing the key MIS 31 and
154 MIS 19 interglacials, and 2) documenting the evolution of the glacial conditions through
155 the Mid-Pleistocene in the MJS. We achieve these goals by reconstructing seawater
156 temperature through and oxygen isotope composition by combining clumped-isotope
157 (Δ_{47}) temperature estimates and $\delta^{18}\text{O}$ measured in foraminifera. In addition, this work
158 will compare Δ_{47} -derived temperatures in benthic foraminifera with Mg/Ca-derived
159 temperatures.

160 Paleodepth reconstructions indicate that the water depth was only a few hundred
161 meters at the time of deposition (D'Alessandro et al., 2003; Stefanelli, 2003; Aiello et al.,
162 2015). Thus, benthic foraminifera in the MJS have recorded sub-surface conditions,
163 characteristic of intermediate waters to upper deep waters. In the rest of this study, we
164 will use the term, “subsurface water”, for hydrographic conditions reconstructed from
165 benthic foraminifers.

166

167 **3. Regional settings and presentation of the Montalbano Jonico Section**

168

169

170 **3.1. Modern oceanographic settings in the Gulf of Taranto**

171

172 The Gulf of Taranto is a semi-enclosed basin, located in southern Italy and open
173 to the Ionian Sea (Figure 1). Its central depth exceeds 2000 m, while coastal areas
174 (continental shelf) are shallower than 200 m. The surface circulation is connected to the
175 Western Adriatic Coastal Current (WACC; Poulain, 2001; Bignami et al., 2007; Turchetto
176 et al., 2007; Goudeau et al., 2014). The WACC has a relatively low salinity due to
177 freshwater runoffs (Turchetto et al., 2007; Pinardi et al., 2016) and shows a clear intra-
178 annual variability. Its influence in the Gulf of Taranto is weaker in summer than in
179 winter and spring because of the reduced river discharges from the Po River and several
180 Alpine and Apennine rivers, leading to a decreased inflow into the Gulf of Taranto during
181 summer (Poulain, 2001; Milligan and Cattaneo, 2007, Brandimarte et al., 2011; Goudeau
182 et al., 2014). In the Gulf of Taranto, waters from WACC are mixed with the Ionian Surface
183 Water (ISW), from the central Ionian Sea (Poulain, 2001; Bignami et al., 2007; Turchetto
184 et al., 2007; Goudeau et al., 2014). The Modified Levantine Intermediate Water (MLIW)
185 can be traced in the basin between 200 and 600 m of water depth (Savini and Corselli,
186 2010). The deeper circulation (below 600 m) in the Gulf of Taranto is influenced by
187 lateral water exchanges with Ionian and Adriatic Sea, which are affected by seasonal
188 changes in the vertical stratification in response to changes in atmospheric dynamics
189 (Turchetto et al., 2007; Civitarese et al., 2010; Cessi et al., 2014; Pinardi et al., 2016).

190 Today, surface-waters show an average temperature around 24 °C and a
191 relatively low and constant salinity of 37.7, which result from the mix between the
192 WACC and the ISW (Figure 3; Poulain, 2001; Bignami et al., 2007; Turchetto et al., 2007;
193 Goudeau et al., 2014; Pinardi et al., 2016). The annually-averaged thickness of the
194 mixed-layer is ~ 50-60m. The thermocline is abrupt, the temperatures decreasing
195 rapidly from 23-24°C at the base of the mixed layer (50-60m) to around 16°C at ~ 100m
196 (Figure 3; Pinardi et al., 2016). The intermediate waters, between 100 and 300m depth,
197 show higher salinities and lower temperatures characteristic of the MLIW (Theocharis
198 et al., 1993; Turchetto et al., 2007). The deeper-water mass shows a low, average
199 temperature around of 14 °C, and a constant salinity of 39 (Figure 3; Pinardi et al.,
200 2016).

201 The carbonate ion concentration [CO_3^{2-}] (Global Alkalinity and Total Dissolved
202 Carbon Estimates Dataset, Goyet et al., 2000) varies from >255 $\mu\text{mol/kg}$ in surface
203 waters to ~ 235 $\mu\text{mol/kg}$ at the base of the 800 m profile shown in Figure 3. These
204 values are high, well above the equilibrium [CO_3^{2-}] values for calcite (varying from 40 to

205 60 $\mu\text{mol/kg}$ over this depth range), indicating that the entire water column is super-
206 saturated with respect to calcite.

207

208 **3.2. The Montalbano Jonico section**

209

210 The Montalbano Jonico Section (southern Italy; $40^{\circ}17'27''\text{N}$, $16^{\circ}33'57''\text{E}$), is
211 located in the Lucania Basin of Bradano Trough (Balduzzi et al., 1982; Casnedi, 1988),
212 between the external border of the Apennines fold and thrust belt and the internal
213 margin of the Apulian Foreland (Figure 1). The Bradano Trough formed in the Early
214 Pliocene and evolved during the Pliocene and Pleistocene. Its inner border experienced
215 deformation associated with polyphasic active thrusts, as a result of interactions
216 between the Apulian Foreland and the Apennines Chain, which determined the north-
217 eastward migration of the Cenozoic Apennine and Pliocene-Pleistocene foredeep units
218 as well as the small-scale marine/lacustrine intramontane basins that were forming at
219 that time (Patacca and Scandone, 2004). The outer margin of the Bradano Foredeep
220 progressively overspread the Mesozoic-Cenozoic Apulian Foreland units (Casnedi et al.,
221 1982).

222 The MJS comprises $\sim 450\text{-m}$ -thick, upward-coarsening deposits ranging from
223 hemipelagic silty clays to silty sands (Figure 2 – Montalbano Jonico composite section).
224 It is interspersed by nine volcanoclastic layers (labelled V1-V9) and five sapropel layers
225 identifiable by benthic foraminiferal and macro-invertebrate assemblages (D'Alessandro
226 et al., 2003; Stefanelli, 2003; Stefanelli et al., 2005; Maiorano et al., 2008).

227 The chronological framework of MJS is based on stable oxygen isotope
228 measurements on benthic ($\delta^{18}\text{O}_b$; *Cassidulina carinata*) and planktonic ($\delta^{18}\text{O}_p$;
229 *Globigerina bulloides*) foraminifera, combined with calcareous plankton biostratigraphy,
230 radiometric dating ($^{40}\text{Ar}/^{39}\text{Ar}$) and identification of sapropel layers (Figure 2). The
231 whole series covers the interval from MIS 37 to MIS 17/16.

232 In the lower part of the section (Interval A; Figure 2), an astronomical age-model
233 was developed by tuning the sapropel layers to precession minima with a constant 3 ka
234 time lag (Ciaranfi et al., 2010; Maiorano et al., 2010), while in the upper part of the
235 section (Interval B; Figure 2), the astronomical tuning was achieved by visual
236 comparison of the MJS $\delta^{18}\text{O}_{\text{planktonic}}$ record to ODP Site 975 $\delta^{18}\text{O}_{\text{planktonic}}$ (Lourens, 2004).
237 The tuning is also supported by glacial-interglacial oscillations observed in $\delta^{18}\text{O}_{\text{benthic}}$ at

238 Montalbano Jonico that can be compared with open ocean benthic stack of Lisiecki and
239 Raymo (2005). Additional tie-points were provided by tephras V3 and V5 precisely
240 dated by $^{40}\text{Ar}/^{39}\text{Ar}$ (Ciaranfi et al., 2010; Maiorano et al., 2010; Petrosino et al., 2015).
241 This chronostratigraphic frame indicates that the MJS covers the time interval from
242 1.240 to 0.645 Ma (Ciaranfi et al., 2010; Figure 2). The estimated sedimentation rates
243 range from 0.28 to 0.9 m/kyr for Interval A and from 0.5 to 2 m/kyr for Interval B
244 (Ciaranfi et al., 2010; Maiorano et al., 2010). The chronostratigraphy of MIS20-MIS19
245 (belonging to Interval B, hereafter referred to as Ideal Section or IS) has been recently
246 improved based on a much higher-resolution benthic foraminifer $\delta^{18}\text{O}$ record (~ 200
247 years resolution) and using a revised $^{40}\text{Ar}/^{39}\text{Ar}$ age of tephra V4 (Nomade et al., 2019).

248

249 **3.3. Paleoenvironmental changes recorded in the MJS**

250

251 **3.3.1. Over the Interval A**

252

253 The major paleoenvironmental changes that occurred during the Interval A of
254 MJS spanning from 1.24 to 0.9 Ma (MIS 37 to 23), were orbitally controlled (Joannin et
255 al., 2008; Girone et al., 2013). Sapropel-like horizons have been described in MJS and
256 their occurrence has been explained by (i) the stratification of the water column and the
257 preservation of organic material at the sea bottom and/or by (ii) enhanced sea surface
258 productivity (Girone et al., 2013). The glacial interglacial cycles through Interval A were
259 considered the result of complex interactions between global climate changes and
260 regional/local responses.

261 In the MJS, MIS 31 limits were set at the mid-slope of MIS 32/31 and of MIS
262 31/30 transition in the benthic foraminifer $\delta^{18}\text{O}$ record, which correspond to 1.095 and
263 1.064 Ma respectively based on the age model of Maiorano et al. (2010). Based on
264 calcareous nannofossil and planktonic foraminifera assemblages, it has been inferred
265 that the MIS 31 corresponds to a long climatic optimum lasting 10 kyr, from 1.075 to
266 1.065 Ma (Girone et al., 2013). Micropaleontological and mineralogical data suggest
267 warm and wet conditions associated with changes in the local precipitation regime with
268 potential effects on sea surface temperature and salinity through enhanced freshwater
269 input into the basin (Stefanelli, 2003; Joannin et al., 2008; Girone et al., 2013). The wet
270 climate likely resulted from strong northern Hemisphere summer insolation associated

271 to precession minimum in a period of high obliquity and eccentricity. This warm climate
272 phase coincided with regional tectonic instability that may have influenced local
273 patterns of erosion and sediment transport (Girone et al., 2013), suggesting that
274 paleoenvironmental changes over MIS 31 at MJS likely result from the interaction
275 between global climate changes and regional factors, in particular associated to
276 landscape evolution.

277

278 **3.3.2. Over the Interval B**

279

280 Interval B (MIS22-MIS17/16) had initially been studied at low resolution with a
281 particular focus on time interval from MIS 20 to MIS 18 (Stefanelli, 2003, 2004; Aiello et
282 al., 2015; Bertini et al., 2015; Toti, 2015; Marino et al., 2015; Maiorano et al., 2016). The
283 chronostratigraphy of MIS 19 benefits from the precise and accurate $^{40}\text{Ar}/^{40}\text{Ar}$ age of the
284 tephra layer V4 (Nomade et al., 2019) as well as from a high-resolution cosmogenic ^{10}Be
285 profile (Simon et al., 2007), a proxy for the dipolar magnetic field intensity that makes it
286 possible to clearly monitor the field weakening associated to the Brunhes-Matuyama
287 magnetic reversal. It also benefits from recent, high-resolution studies of marine
288 microfossils and pollen assemblages (Aiello et al., 2015; Bertini et al., 2015; Marino et al.,
289 2015; Maiorano et al., 2016), and from high-resolution records of benthic $\delta^{18}\text{O}$ and $\delta^{13}\text{C}$
290 changes recently obtained over the MIS 20-MIS 18 interval (Nomade et al., 2019). This
291 set of data provides invaluable pieces of information about the climatic and
292 environmental variability throughout the MIS 19.

293 The deglaciation between MIS 20 and MIS 19 (Termination IX) is characterized by the
294 cyclic advection of cold surface waters that likely originated from the North Atlantic and
295 resulted in an “Heinrich-like event” followed by a potential “Bølling-Allerød-like event”
296 and a “Younger Dryas-like event” (Maiorano et al., 2016). During MIS19c, several proxies
297 point to the existence of a shallow-water analogue to a sapropel event (Maiorano et al.,
298 2016). This so-called “red interval” or “ghost sapropel” (Emeis et al., 2000), seems to
299 correspond to the “i-cycle 74” event according to Lourens, (2004). The existence of a
300 shallow-water sapropel is supported (i) by a negative excursion in benthic foraminifera
301 $\delta^{13}\text{C}$, which suggests an enhanced stratification of the upper water column and/or an
302 increased productivity (Nomade et al., 2019), and which is coeval with (ii) a low oxygen
303 content at the sediment-water interface (Stefanelli, 2003). During this event, marine

304 (Maiorano et al., 2016) and continental (Bertini et al., 2015) proxies suggest an increase
305 in sea-surface temperatures (SST) and a climatic amelioration on land with a rapid
306 increase in annual precipitation, both of which providing favourable conditions for
307 sapropel formation during an insolation maximum (Maiorano et al., 2016; Nomade et al.,
308 2019). The MIS 19c is associated with warm and wet conditions in continual and warm
309 surface waters (Bertini et al., 2015; Maiorano et al., 2016 and Nomade et al., 2019).

310

311 **4. Materials and methods**

312

313 **4.1. Conventional stable isotope analyses**

314

315 Planktonic and benthic foraminifera were handpicked for stable isotope analyses.
316 Around 20-30 individuals of *Globigerinoides ruber* and *Cassidulina carinata* and 7-15
317 individuals for *Uvigerina mediterranea* and *Elphidium crispum*, were picked from the
318 200-355 μm fraction. The three-benthic species (*U. mediterranea*, *C. carinata* and *E.*
319 *crispum*) are shallow infaunal or epifaunal species (Altenbach et al., 1999; Fontanier et
320 al., 2002; Murray, 2006), which can live on different substrates, such as on sand or on
321 algae (Murray, 1963). From 1 to 5 replicate analyses of $\delta^{18}\text{O}$ and $\delta^{13}\text{C}$ were performed.
322 Foraminifera were cleaned in an ultrasonic bath for few seconds with reagent-grade
323 methanol to eliminate impurities. $\delta^{18}\text{O}_{\text{VPDB}}$ and $\delta^{13}\text{C}_{\text{VPDB}}$ values were measured at the
324 Laboratoire des Sciences du Climat et de l'Environnement (LSCE) using a MultiCarb
325 system coupled to a dual-inlet Isoprime (Elementar). Standardization to VPDB was
326 based on repeated measurements of international reference materials NBS 19 and NBS
327 18, with respective nominal values for $\delta^{18}\text{O}_{\text{VPDB}}$ of -2.20 ‰ and -23.01 ‰, and for
328 $\delta^{13}\text{C}_{\text{VPDB}}$ of 1.95 ‰ and -5.01 ‰. The uncertainties reported here are based on the
329 external reproducibility of an in-laboratory carbonate standard (MARGO) with 1SD =
330 0.05 ‰ for $\delta^{18}\text{O}_{\text{VPDB}}$ and 1SD = 0.03 ‰ for $\delta^{13}\text{C}_{\text{VPDB}}$.

331

332 **4.2. Clumped-isotope analyses**

333

334 Clumped-isotope method is a promising isotopic thermometer for seawater
335 paleo-reconstructions because 1) it does not require that one knows the past isotopic
336 composition of seawater, $\delta^{18}\text{O}_{\text{sw}}$ (Schauble et al., 2006) and 2) there are no detectable
337 vital or salinity effects for both the planktonic and the benthic foraminifera Δ_{47} (Tripathi

338 et al., 2010; Grauel et al., 2013; Peral et al., 2018). The main limitation is analytical. From
339 2 to 3 mg of foraminifer calcite are required in order to perform one clumped isotope
340 measurement and a minimum of four replicates are mandatory to reduce significantly
341 the analytical uncertainty. In the Montalbano Jonico section, large amounts of thick and
342 heavy benthic foraminifer shells were available for Δ_{47} replicate analyses, but planktonic
343 foraminifera were not present in large enough quantities to reconstruct SST with the
344 clumped-isotope thermometer.

345 A total of 257 clumped-isotope analyses were performed at the LSCE, including
346 143 measurements on benthic foraminifera from Interval A and B, and 114
347 measurements of carbonate standards. We combined different foraminifer size fractions
348 and cleaned benthic foraminifera with water and methanol after crushing, following the
349 protocol described by Peral et al. (2018). Each carbonate sample was then weighed and
350 between 2 and 3 mg were dissolved in a common phosphoric acid bath at 90°C during
351 15 min. The resulting CO₂ was purified in an automated line by cryogenic trapping to
352 remove water and passed through a Porapak Q column at -20 °C under helium 6.0 flow.
353 This CO₂ was transferred by gas expansion into an Isoprime 100 dual-inlet mass
354 spectrometer (Daëron et al., 2016). Conversion of Δ_{47}^{raw} to absolute Δ_{47} values was done
355 using carbonate standards (ETH-1/2/3; Meckler et al., 2014; Bernasconi et al., 2018),
356 and processed using the IUPAC isotopic parameters (Brand et al., 2010) following the
357 procedure described by Daëron et al. (2016). “Absolute” Δ_{47} values were then converted
358 to temperatures using the calibration of Peral et al. (2018).

359 Where possible, three species of benthic foraminifera were picked from each
360 sample (i.e. same stratigraphic depth), *Uvigerina mediterranea* (200-355 μm),
361 *Cassidulina carinata* (200-315 μm) and *Elphidium crispum* (200-450 μm ; only for one
362 stratigraphic level). From 2 to 27 replicates for each sample/species pair were done in 4
363 sessions of measurements between July 2016 and June 2018. The first session (2016-
364 07) and the last one (2018-05) were corrected for a slow trend observed in the
365 measured Δ_{47} values of ETH-3, probably resulting from subtle changes in the ion
366 collector backgrounds. Each analytical session (defined as continuous period of Δ_{47}
367 measurements) was assigned an independent external Δ_{47} reproducibility (respectively
368 15.9 ppm, 13.9 ppm, 20.9 ppm and 18.1 ppm at 1SE) based on repeated analyses of
369 standards and samples. Details about the data processing are given with the python
370 routine provided in the supplementary material.

371
372
373

4.3. Analyses of Mg/Ca ratio

374

375 Mg/Ca measurements were performed at LSCE on planktonic and benthic
376 foraminifera. A minimum of 30 foraminifera (~ 250 µg) were hand-picked in the size
377 range between 250 and 355 µm and cleaned following the Barker et al. (2003) protocol.
378 Shells were crushed between two glass plates and the resulting fragments were put into
379 micro-vials, making it possible to wash out fine material (i.e. clay) through repeated
380 cleaning with purified water and then ethanol. In order to remove potential organic
381 contaminants, the samples were then oxidized with alkali-buffered 1% H₂O₂ solution for
382 10 minutes at 100°C. The final cleaning treatment consists in a rapid leaching with 0.001
383 M HNO₃. After dissolution in HNO₃ 0.075 M, each sample was analysed by inductively
384 coupled plasma mass spectrometry (ICP-MS), using a PlasmaQuant ELITE system from
385 Analytik Jena. After a preliminary run to estimate the Ca concentrations, samples were
386 then diluted to a uniform Ca concentration of around 100 ppm. Mg/Ca ratios were
387 accurately determined following the intensity ratio method (De Villiers et al., 2002). The
388 calibration standards were prepared from single element solutions (e.g. Ca, Sr, Mg).
389 Mg/Ca instrumental precision was determined based on multiple replicates of a
390 standard solution of known Mg/Ca composition. It averages ± 1.3 %, with daily
391 variations varying from 0.9 to 1.6%.

392 The Mg/Ca ratios were measured on the planktonic foraminifera *G. ruber* and on
393 the benthic foraminifera *U. mediterranea*. The Mg/Ca ratios were converted to
394 temperature using species-specific calibrations:

395 - For *G. ruber*: we used the calibration of Anand et al. (2003)

396

$$397 \quad T = \log \left(\left(\frac{Mg/Ca}{0.449 (\pm 0.06)} \right) / 0.09 \right) \quad (1)$$

398

399

400 - For *U. mediterranea*: we used the calibration of Elderfield et al. (2010)

401

$$402 \quad T = \log \left(\left(\frac{Mg/Ca}{0.86 (\pm 0.05)} \right) / 0.07 (\pm 0.005) \right) \quad (2)$$

403

404
405 where T (in °C) is the temperature.
406 The uncertainties were calculated by propagating the analytical errors, based on the
407 long-term standard deviation of our standards and uncertainties associated with
408 calibrations.

409 410 4.3.1. Calibration and potential biases

411
412 Several potential sources of uncertainties or leading to systematic errors have been
413 reported for Mg/Ca-thermometry in foraminifer shells. First, Mg/Ca-T calibration
414 exercises have revealed species-dependent differences and/or size effects for
415 foraminifers (Anand et al., 2003) and inter-laboratory comparisons have shown the
416 existence of significant offset (up to 14%) associated to the cleaning protocol (Rosenthal
417 et al., 2007). Thus, in the present work, we have used species-specific Mg/Ca-T
418 calibrations that were obtained with the same cleaning protocol that we used (i.e. Anand
419 et al, 2003 for *G. ruber* in the 250-350 μ m size fraction, and Elderfield et al., 2010 for *U.*
420 *mediterranea*).

421 Recent calibrations have also suggested that Mg/Ca in foraminifer shells is not only
422 temperature dependent but could be also affected by salinity (Nurnberg et al., 1996; Lea
423 et al., 1999; Ferguson et al., 2008; Kisakurek et al., 2008; Mathien-Blard and Bassinot,
424 2009; Arbuszewski et al., 2010; Gray et al., 2018) and/or pH or CO₃⁼ (Russell et al.,
425 2004; Kisakurek et al., 2008; Elderfield et al., 2006; Gray et al., 2018). However, because
426 we cannot estimate accurately salinity and pH variations along the MPT interval, no
427 effort was made in the present paper to take these effects into account.

428 429 5. Results

430 431 5.1. $\delta^{18}\text{O}_{\text{vpdb}}$ measurements

432
433 $\delta^{18}\text{O}_{\text{VPDB}}$ and $\delta^{13}\text{C}_{\text{VPDB}}$ measurements were performed on 3 species of benthic
434 (*Cassidulina carinata*, *Elphidium crispum* and *Uvigerina mediterranea*) and one species of
435 planktonic foraminifera (*Globigerinoides ruber*), except for sample DFJ-27/29 (transition
436 between MIS 22 and MIS 21) and the older two samples (FG-39/40 and FG-10/11) in
437 which *G. ruber* specimens were not present in sufficient quantity. All the measurements
438 are presented in supplementary material Table S1.

439 The difference of $\Delta^{18}\text{O}_c$ between the three species of benthic foraminifera ranges
440 between 0 and 0.43 ‰ (Table 1), which is larger than the internal analytical uncertainty
441 (± 0.05 ‰). Since the good reproducibility of replicate measurements suggests
442 homogeneous samples, the observed differences likely result from the so-called “vital”
443 effects. But our results are puzzling since, according to Grossman (1987), both *Uvigerina*
444 spp. and *Cassidulina* spp. are believed to precipitate following the equation of Kim and
445 O’Neil (1997). The range of differences and the small number of intervals studied here
446 do not allow us to quantify precisely the species-specific, oxygen-18 differences between
447 *C. carinata*, *U. mediterranea* and *E. crispum*.

448 Variations in the difference between benthic species and the planktonic species *G.*
449 *ruber* ($\Delta^{18}\text{O}_{c(p vs b)}$, hereafter) are larger than the inter-benthic variability, and are, as
450 expected, primarily driven by changes in the planktonic $\delta^{18}\text{O}$ values. $\Delta^{18}\text{O}_{c(p vs b)}$ values
451 remain relatively constant for glacial periods (MIS 36, 34, 30 and 20), hovering between
452 1.37 and 1.86 ‰, except for sample DFJ-23 (MIS 22), which yields ~ 2.5 ‰, a value
453 comparable to those for interglacial periods. By contrast, a much larger variability is
454 observed for the interglacial periods (MIS 31, 21 and 19), with benthic-planktonic
455 differences ($\Delta^{18}\text{O}_{c(p vs b)}$) ranging between 1.32 and 3.19 ‰ (Table 1).

456

457 5.2. Temperatures estimated from clumped-isotope measurements

458

459 Final Δ_{47} values and the corresponding temperature reconstructions are given in
460 Table 2. More details in the data processing (python code) and all the Δ_{47} measurements
461 are presented in supplementary material Table S2. Given the analytical standard
462 deviation, the Δ_{47} -derived temperatures for *U. mediterranea* and *C. carinata* are
463 statistically indistinguishable from each other in samples NC-199, DFJ-57, FG-39/40 and
464 FG-10/11. The absence of species-specific effects in clumped isotopes (Tripathi et al.,
465 2010; Grauel et al., 2013; Peral et al., 2018) allows us to combine results from the three
466 benthic species to compute average Δ_{47} -derived temperatures and reduce the analytical
467 error. By doing so, we assume that there is no significant temperature difference
468 between the water-sediment interface (epifaunal species habitat) and the first
469 centimetres of sediments where the infaunal species grew. An additional assumption is
470 that bioturbation does not result in large vertical remobilisation that could have brought
471 together benthic specimens from different climatic intervals. The high sedimentation

472 rates of MJS and the large quantity of material required for Δ_{47} measurements insure
473 that the effects of vertical remobilisation can be neglected.

474 The reconstructed glacial temperatures range from 7.1 °C (\pm 3.6 °C, 2SE) to
475 12.1 °C (\pm 4.2 °C, 2SE), for samples NC-172, DFJ-72, DFJ-23, DFJ-20, FG-103/104 and FG-
476 124, while interglacial temperatures are warmer, with a lower variability, respectively
477 14.8 °C (\pm 2.6 °C, 2SE) and 16.6 (\pm 3 °C, 2SE) for MIS 19 (sample NC-271) and MIS 21
478 (DFJ-57). Surprisingly, two of the three Δ_{47} -derived temperature values obtained during
479 MIS31 (samples FG-103/104 and FG-119/121) are similar to the glacial period
480 temperatures and only the last sample (FG-124), within the $\delta^{18}\text{O}$ optimum of MIS31,
481 shows a warm temperature of 13.8 °C (\pm 3 °C, 2SE). It is worth noting that samples DFJ-
482 27-29 and NC-172, located at the transitions between MIS 22 – MIS 21 and between MIS
483 20 – MIS 19, yield significantly different temperatures, 8.6 °C (\pm 3.8 °C, 2SE) and 12.1 °C
484 (\pm 1.6 °C, 2SE; Table 2), respectively.

485

486 **5.3. Temperatures estimated from Mg/Ca ratio measurements**

487

488 Our study makes it possible to compare Mg/Ca-thermometry to clumped-isotope
489 paleotemperatures. All the Mg/Ca analyses on benthic foraminifers were performed on
490 the species *U. mediterranea*. For a few samples in which enough planktonic shells were
491 available, we also reconstructed Mg/Ca-derived sea-surface temperatures (SST
492 hereafter) using the planktonic foraminifer *G. ruber*. All the Mg/Ca results are provided
493 in supplementary material Table S3 and summarized in Table 3.

494 Monitoring Al/Ca, Fe/Ca and Mn/Ca makes it possible to check for potential
495 contaminations. The low values Mn/Ca and Al/Ca and the lack of any clear correlation
496 between these elemental ratios and Mg/Ca values (Figure 4) suggest that our Mg/Ca
497 dataset is neither affected by Mn-rich oxides nor clay material. Only one sample (DFJ-72)
498 showed an unusually high Al/Ca ratio, but it is not associated with an anomalous Mg/Ca
499 ratio (Figure 4). The Fe/Ca values are relatively high in our samples (Figure 4), but
500 without any noticeable impact on Mg/Ca. We suspect that the Fe values could reflect the
501 presence of small amounts of pyrite, which is not removed by our cleaning protocol.
502 Sample FG-119/121 was analysed twice because the first results yielded an unrealistic
503 benthic Mg/Ca-temperature of 28.6 °C (\pm 3.4 °C, 2SE), warmer than the Mg/Ca-derived
504 SST obtained in the same sample on *G. ruber* (22.7 ± 1.8 °C, 2SE; Table 3). Although there

505 was no indication of detrital or oxide contamination, we decided to re-analyse this
506 sample after adding another leaching step to our cleaning protocol. The second set of
507 replicates yield a bottom water temperature of 20.9 °C (± 3.0 °C, 2SE) for this sample.

508 Through the Interval A, as expected, Mg/Ca-derived SSTs indicate colder
509 temperatures during the glacials MIS 36 (FG-10/11 and FG-39/40), MIS 34 (FG-74) and
510 MIS 30 (IMJ-5b) than during interglacial MIS 31 (FG-103/104, FG-119/121 and FG-124).
511 Along the interglacial MIS 31, SSTs increase from 22.5 to 24.7 °C. As far as benthic
512 foraminifer results are concerned, glacial Mg/Ca-derived sub-surface water
513 temperatures are in good agreement with our Δ_{47} -derived temperature estimates. By
514 contrast, in interglacial MIS 31, Mg/Ca-derived temperatures obtained from *U.*
515 *mediterranea* are higher than the corresponding Δ_{47} -derived temperatures.

516 In the Interval B, Mg/Ca-SSTs vary less in Interval B than interval A, ranging
517 between 20.8 °C (± 1.8 °C, 2SE) and 23.1 °C (± 1.6 °C, 2SE). Two samples, however, show
518 much warmer temperatures: NC-199 (transition from MIS 20 and 19), with a SST of
519 27.8 °C (± 1.8 °C, 2SE) and sample NC-271 (MIS 19) with a SST of 25.4 °C (± 1.6 °C, 2SE;
520 Table 3). As far as bottom water temperature are concerned, Mg/Ca-reconstructed
521 temperatures range from 9.7 to 18.2 °C. Surprisingly, the glacial periods yield warmer
522 bottom temperatures than the interglacials: the two glacial MIS 22 samples yield high
523 bottom temperatures of 18.2 °C (± 2.6 °C, 2SE) and 17.2 °C (± 2.4 °C, 2SE), and in MIS 20
524 bottom temperatures are 14.1 °C and 14.7 °C (± 2.2 °C, 2SE). The deglaciation samples
525 show Mg/Ca temperatures comparable to those derived from Δ_{47} , with 9.7 °C (± 1.8 °C,
526 2SE) for MIS 22-21 and 14.7 °C (± 2.2 °C, 2SE) for MIS 20-19. Bottom water
527 temperatures for interglacial periods are indistinguishable, within analytical
528 uncertainties, from Δ_{47} -derived estimates: 11.9 °C (± 1.4 °C, 2SE) for MIS 21 and 12.9 °C
529 (± 1.6 °C, 2SE) for MIS 19 (Table 3).

530

531

532 **5.4. Subsurface seawater $\delta^{18}\text{O}$ reconstruction**

533

534 The subsurface seawater $\delta^{18}\text{O}$ ($\delta^{18}\text{O}_{\text{sw}}$, hereafter) derived from paired Δ_{47} - $\delta^{18}\text{O}_{\text{c}}$ data
535 are presented in Table 4. We paired our Δ_{47} -derived temperature estimates with the
536 corresponding $\delta^{18}\text{O}_{\text{c}}$ values of each benthic species, using the $^{18}\text{O}/^{16}\text{O}$ fractionation
537 relationship of Kim and O'Neil (1997):

538
$$1000 \ln(\alpha_{CC/W}) = 18.03 \times 1000 / T - 32.17 \quad (3)$$

539 where T is temperature in ° Kelvin (K) and $\alpha_{CC/W}$ is the oxygen-18 fractionation factor
540 between calcite and water: $\alpha_{CC/W} = (1 + \delta^{18}O_{C/VSMOW} / 1000) / (1 + \delta^{18}O_{SW/VSMOW} / 1000)$
541 with $\delta^{18}O_{C/VSMOW}$ and $\delta^{18}O_{SW/VSMOW}$ corresponding to foraminiferal calcite and seawater,
542 respectively, both relative to VSMOW.

543 Reconstructed $\delta^{18}O_{SW}$ values range from 0.7 ‰ (± 0.6 ‰ 2SE) to 3.0 ‰ (\pm
544 0.4 ‰ 2SE), with higher values during glacial than during interglacials through the
545 Interval A. Within MIS 31 the $\delta^{18}O_{SW}$ values are relatively low (1.0 ‰ \pm 0.6 ‰, 2SE) for
546 sample FG-103/104, and 0.7 ‰ (± 0.6 ‰, 2SE) for sample FG-119/121 but increase to
547 2.0 ‰ (± 0.6 ‰, 2SE) in sample FG-124. In the interval B, changes between interglacial
548 and glacial periods are small and remain within the range of propagated analytical
549 uncertainties.

550

551 **6. Discussion**

552

553 **6.1. Clumped Isotope versus Mg/Ca-derived Temperatures**

554

555 As indicated above, the comparison of the two thermometers can only be
556 achieved for benthic foraminifers since we could not extract enough planktonic shells
557 for clumped-isotope analyses. Within Interval A of MJS, throughout the three glacial
558 periods we investigated, both thermometers yield very similar temperature estimates
559 (Figure 5.a). By contrast, during interglacial MIS 31, Mg/Ca-derived temperatures are
560 significantly higher than those derived from Δ_{47} . The first set of analyses on sample FG-
561 119/121 (MIS 31) resulted in an unrealistic benthic Mg/Ca-derived temperature ($28.6 \pm$
562 3.4 °C, 2SE), warmer than the Mg/Ca-derived SST values obtained in the same sample on
563 *G. ruber* (22.7 ± 1.8 °C, 2SE; Table 3). We re-analyzed this sample and the second set of
564 data yielded a cooler benthic temperature (20.9 ± 3.0 °C 2SE), although still much
565 warmer than the corresponding Δ_{47} estimate (8.1 ± 2.6 °C 2SE).

566 For the Interval B, the Mg/Ca-derived temperatures do not show significant
567 changes between glacial and interglacial periods (Figure 5.b). By contrast, Δ_{47}
568 temperatures display larger variations correlated with benthic foraminifer $\delta^{18}O$
569 oscillations. The Mg/Ca-derived temperatures are higher than the Δ_{47} -derived ones
570 during glacial periods, and lower during interglacial periods.

571 The Mg/Ca-derived temperatures during glacials such as for instance those in
572 MIS22 (i.e. 18.2 ± 2.6 °C (2SE) and 17.2 ± 2.4 °C (2SE)) are not only higher than Δ_{47}
573 results, they also correspond to temperatures only found today at very shallow water
574 depths (~ 100 m) in the Gulf of Taranto (Pinardi et al., 2016; Figure 3). The difference
575 between benthic and planktonic $\delta^{18}\text{O}$ (which vary from $\Delta\delta^{18}\text{O}_{c(p\text{ vs }b)} = 1.75$ to $\Delta\delta^{18}\text{O}_{c(p\text{ vs }b)}$
576 $= 2.51$ in interval B) rule out the possibility that the deposition site could have been
577 located under such a shallow water depth. As seen above, trace elements, used to
578 monitor potential contaminations (i.e. Mn, Fe, Al), do not reveal any oxides
579 contamination or presence of detrital material. Even sample FG-119/121, for which a
580 first set of results yielded a clearly anomalous bottom water temperature of 28.7°C (\pm
581 3.4 °C, 2SE; warmer than the Mg/Ca-derived surface temperature obtained on the same
582 sample) did not show anomalous Mn, Fe or Al contents (Figure 4).

583 It has been shown from recent studies of core-top material that the Mg/Ca-
584 thermometer in the Mediterranean Sea can be affected by the growth of Mg-rich calcite
585 precipitated on foraminifer shells during early diagenetic processes (Boussetta et al.,
586 2011; Sabbatini et al., 2011). The development of diagenetic calcite has been attributed
587 to the super-saturation of Mediterranean bottom water [$\text{CO}_3^{=}$] with respect to calcite.
588 However, if such a diagenetic mechanism was at play, it would affect both benthic and
589 planktonic shells. In general, Mg/Ca-derived temperatures performed on planktonic
590 shells do not result in unrealistic SST values (assuming that past values should be in the
591 same range as modern values), with the exception of sample NC-172. Thus, it is not clear
592 whether anomalous Mg/Ca-derived sub-surface temperatures could be attributed to a
593 diagenetic effect. Alternatively, several studies have concluded that the Mg/Ca-
594 thermometer on foraminifers can be biased by salinity and/or pH (Russell et al., 2004;
595 Elderfield et al., 2006; Raitzsch et al., 2008; Kisakurek et al., 2008; Mathien-Blard and
596 Bassinot, 2009; Gray et al., 2018). Modern geochemical profiles show that $\text{CO}_3^{=}$
597 concentrations in the Gulf of Taranto (and in most of the Mediterranean Sea) are much
598 higher than in open ocean areas (Figure 3). Yet, without estimates of pH or [$\text{CO}_3^{=}$]
599 variations along the Mid-Pleistocene in the Mediterranean Sea one has no possibility to
600 conclude about pH or carbonate ion influences on the Mg/Ca-thermometer in MJS. As far
601 as a potential salinity effect is concerned, benthic-derived $\delta^{18}\text{O}_{\text{SW}}$ values from paired Δ_{47} -
602 $\delta^{18}\text{O}$ do not show a clear relationship with Mg/Ca-temperatures but uncertainties are
603 too large to drive any robust conclusion.

604 One cannot exclude also the possibility that the Mg/Ca ratio of waters in the Gulf
605 of Taranto did not remain constant through time owing to the semi-enclosed nature of
606 the basin, which may make it sensitive to continental rock weathering and local river
607 runoffs. The Mg/Ca-thermometry is based on the assumption that Mg/Ca in seawater is
608 constant and invariant through time. This assumption is likely to be true in open oceans
609 due to the long residence time of Mg and Ca, respectively 13 Ma and 1 Ma (Broecker and
610 Peng, 1982; Brunland, 1983; Riley and Skirrow, 1975). However, seawater Mg/Ca may
611 have varied through time in the Gulf of Taranto due to local inputs of dissolved Mg and
612 Ca from nearby river runoffs. Why such changes may have affected preferentially sub-
613 surface Mg/Ca records is not clear, though, and we have no possibility to address that
614 potential source of bias for Mg/Ca-thermometry.

615 In conclusion, we cannot rule out the possibility that discrepancies we observed in
616 several intervals between benthic Mg/Ca- and Δ_{47} -derived temperatures reflect changes
617 in the chemistry of bottom waters and/or diagenetic effects but given the observation
618 available in the present paper none of the above hypotheses can be tested with
619 confidence. Further studies are mandatory to address those anomalously high Mg/Ca-
620 derived sub-surface temperatures in MJS. For the rest of this manuscript, we have
621 decided to favour Δ_{47} -derived subsurface temperatures for our palaeoceanographic
622 interpretations owing to the fact that in the present state of our current knowledge,
623 there is no strong bias known for the clumped-isotope thermometer whereas several
624 studies have highlighted potential problems for the Mg/Ca-thermometry in the
625 Mediterranean Sea (Ferguson et al., 2008; Boussetta et al., 2011; Sabbatini et al., 2011).
626 But those issues about Mg/Ca biases are not agreed upon by the whole community,
627 several recent works concluding about the quality and consistency of Mg/Ca-derived
628 temperatures in the Mediterranean Sea (e.g. Cisneros et al., 2016; Catala et al., 2019).

629 In the present paper, although we favour clumped-isotope temperatures for benthic
630 foraminifers, we have no alternative than using Mg/Ca-derived temperatures for sea-
631 surface conditions (planktonic data).

632

633 **6.2. Paleocceanographic conditions during the glacial periods**

634

635 We propose firstly to describe the evolution of the glacial periods through the
636 MPT at MJS (Figure 6) in term of water-column stratification and sub-surface water

637 temperatures and $\delta^{18}\text{O}_{\text{sw}}$. To the best of our knowledge, our results provide the first
638 sub-surface temperature and $\delta^{18}\text{O}_{\text{sw}}$ reconstructions for the five Mid-Pleistocene glacial
639 periods MIS 36, 34, 30, 22 and 20 in the central Mediterranean Sea.

640

641 **6.2.1. Glacial conditions within Interval A**

642

643 Δ_{47} -derived temperature estimates are low (between $8.0\text{ }^{\circ}\text{C} \pm 2.4\text{ }^{\circ}\text{C}$ and $11.2\text{ }^{\circ}\text{C} \pm$
644 $3.2\text{ }^{\circ}\text{C}$ at 2SE; Table 2; Figure 6) within the Interval A. Such values are much cooler than
645 temperatures that can be found today in the upper water column of the Gulf of Taranto
646 (Pinardi et al., 2016, Figure 3).

647 Paired Δ_{47} - $\delta^{18}\text{O}$ data obtained on specific-benthic species were used to
648 reconstruct past $\delta^{18}\text{O}$ of sub-surface seawater. As expected, the glacial seawaters are
649 oxygen-18-enriched relative to the interglacial MIS 31 values, likely reflecting the fact
650 that more water is stored in continental ice sheets during these glacial periods than
651 during MIS 31 (Figure 6).

652 The difference of $\delta^{18}\text{O}_c$ between the surface (planktonic foraminifera) and sub-
653 surface (benthic foraminifera; $\Delta^{18}\text{O}_c$ (p vs b)) can be used to address the vertical
654 stratification (Zahn et al., 1991). Lower $\Delta^{18}\text{O}_c$ (p vs b) values are observed for glacial
655 periods (MIS 34 and 30) compared to those for MIS 31, which argues for a more efficient
656 vertical mixing during glacial periods (Figure 6).

657 The reconstructions of land conditions are based on pollen and can be
658 summarized by the use of the ratio between two groups of taxa: mesothermic and
659 steppic taxa. This ratio makes it possible to discriminate between warm-temperate
660 periods (mesothermic dominance) and cold periods (steppic dominance; Figure 7;
661 Joannin et al., 2008). One of the most abundant local taxa is the mesophilous deciduous
662 tree *Quercus*, which is also the most representative taxon of the mesothermic plants
663 recorded through the Interval A (Joannin et al., 2008). This taxon suggests that warm-
664 temperate periods are also humid (Rossignol-Strick and Paterne, 1999). Several
665 warm/temperate and wet phases characterized by the dominance of mesothermic
666 groups are highlighted during the interglacial periods through the Interval A, while the
667 glacial periods are characterized by much colder and drier climates (i.e. dominance of
668 steppic elements; Figure 7). Changes in the relative abundance of tropical-subtropical
669 marine planktonic species (Figure 7; Girone et al., 2013) suggest that warm surface

670 conditions (i.e. increased abundance of *G. ruber* and *Globigerinoides tenellus*) were
671 associated to warm periods on land (Joannin et al., 2008), and drifted slowly to cooler
672 conditions at the onset of glacial periods. The glacial MIS 30 is characterized by an
673 abrupt decrease of tropical-subtropical planktonic species indicating colder conditions
674 (Figure 7; Girone et al., 2013), compared to the previous warm MIS 31. The evolution of
675 the mesothermic vs. steppic ratio suggests cold and dry climate that may have
676 significantly reduced the river runoff and resulted in saltier waters in the Gulf of Taranto
677 (high $\delta^{18}\text{O}_{\text{sw}}$; Figure 6), thus making the upper water column more prone to vertical
678 mixing during the glacial periods. This agrees with the higher glacial $\delta^{13}\text{C}_{\text{planktonic}}$ values
679 which may reflect increased surface productivity made possible by the enhanced
680 vertical mixing and the upward redistribution of nutrient-enriched sub-surface waters
681 (Figure 2; Brilli, 1998).

682

683

684 **6.2.2. Glacial conditions within Interval B**

685

686 The two samples from MIS 22 provide contrasting pieces of information despite
687 having been retrieved close to one another in the MJS. The older sample (DFJ-20) is
688 characterized by a relatively warm sub-surface Δ_{47} -temperature (12.1 ± 5.2 °C at 2 SE)
689 (Figure 6). For this stratigraphic level, the $\Delta^{18}\text{O}_{\text{c (p vs b)}}$ is small, suggesting a good vertical
690 mixing (Figure 6). The second sample (DFJ-23), retrieved in the peak maximum of $\delta^{18}\text{O}$,
691 reveals a colder sub-surface Δ_{47} -temperature (9.4 ± 1.9 °C). In this sample, $\Delta^{18}\text{O}_{\text{c (p vs b)}}$ is
692 high, implying a more pronounced stratification of the water column (Figure 6). Changes
693 in sub-surface temperature reconstructed from benthic Δ_{47} appear coherent with
694 vertical mixing history reconstructed from $\Delta^{18}\text{O}_{\text{c (p vs b)}}$, with lower sub-surface
695 temperature when stratification is stronger and higher sub-surface temperature
696 associated to more active vertical mixing. Yet, one cannot rule out the possibility that
697 sub-surface temperature history is also controlled to some extent by lateral advection of
698 thermocline water of Ionian or Adriatic origins (Pinardi et al., 2016).

699 The glacial MIS 20 is characterized by cold, sub-surface Δ_{47} -derived temperatures
700 and some vertical mixing of the column water (as evidenced by the low $\Delta^{18}\text{O}_{\text{c (p vs b)}}$
701 gradient; Figure 6). These observations, combined with the constant and high value of
702 $\delta^{18}\text{O}_{\text{b}}$ (Figure 8; Nomade et al., 2019), suggest that the climatic conditions during the MIS

703 20 were relatively cold and stable. The late MIS 20 (change between samples NC-172
704 and NC-199) corresponds to a -0.25‰ decrease of $\delta^{18}\text{O}_{\text{benthic}}$ (Figure 8). This would be
705 equivalent to a temperature increase of $\sim 1\text{ °C}$, assuming a constant $\delta^{18}\text{O}_{\text{sw}}$. However,
706 clumped isotopes indicate that the bottom water temperatures increased by $\sim 5\text{ °C}$
707 (Figure 6 and 8) between the two studied samples. This implies that that the shift in
708 $\delta^{18}\text{O}_{\text{b}}$ actually reflects the combined effects of a temperature increase and a 1 ‰
709 increase of water $\delta^{18}\text{O}_{\text{sw}}$. SSTs derived from foraminiferal and nannofossil assemblages
710 (PC1 nannofossil and foraminifera) suggest persistent and cold surface water
711 temperatures across the MIS 20 (Figure 8). These low temperatures are evidenced by
712 the high abundance of the polar-subpolar species *Neogloboquadrina pachyderma* left
713 coiling (Figure 8) and *Coccolithus pelagicus* ssp. *pelagicus* (Maiorano et al., 2016). The
714 strong stratification that persisted despite the relative warming of sub-surface
715 temperatures suggests that the increase of $\delta^{18}\text{O}_{\text{sw}}$ could correspond to the lateral
716 advection of saltier (and warmer) sub-surface water at the end of MIS 20.

717

718 **6.2.3. Evolution of glacial conditions through the Mid-Pleistocene Transition**

719

720 As seen above, in interval A the glacial periods we studied show similar
721 conditions characterized by high $\delta^{18}\text{O}_{\text{sw}}$ ($\sim 1.7\text{ ‰}$) and cold ($\sim 9\text{ °C}$) sub-surface
722 temperatures in a context of well-mixed water column (Figure 6). In Interval B, glacial
723 periods are slightly more variable (Figure 6). The hydrographic conditions during
724 MIS 20 are similar to those occurring during glacial periods of Interval A. The two
725 nearby samples analysed in MIS 22 suggest, however, the possibility of some variability
726 during glacials with the penultimate MIS22 sample showing a surprisingly warmer
727 temperature (12.1 °C) than the MIS22 sample that was retrieved in the maximum $\delta^{18}\text{O}$
728 peak (9.4 °C ; Figure 6). When averaging out these two MIS22 temperatures, the mean
729 value is slightly higher than in the other glacials studied in MJS. While the MIS22 is often
730 seen in many open ocean $\delta^{18}\text{O}$ records as one of the first intense post-MPT glacials, it
731 seems to be characterized by anomalously warmer sub-surface temperatures compared
732 to other Mid-Pleistocene glacial periods in the Gulf of Taranto (Figure 6).

733 The paleo-water depth reconstruction (Figure 6) suggests that water depth
734 varied from bathyal through Interval A to circalittoral through Interval B due to tectonic
735 uplifting (Stefanelli, 2003). If the structure of the water column had remained roughly

736 similar to today, we would expect that such a major shallowing of the deposition site
737 would have resulted in much warmer sub-surface (benthic) temperatures and reduced
738 planktonic-benthic differences. This is not what is observed in the data. Within the limit
739 of our error uncertainties, sub-surface (benthic) water temperatures and $\delta^{18}\text{O}_{\text{sw}}$ appear
740 to be rather constant and undistinguishable between all the studied glacials throughout
741 intervals A and B (with the exception of one sample in MIS22). The absence of any clear
742 temperature increase may either suggest that the tectonic uplift was more limited than
743 previously thought and/or that the benthic temperature increase resulting from the
744 shallowing of the site had been counterbalanced by an overall cooling of the water
745 column in interval B compared to interval A.

746

747 **6.3. Paleoceanographic conditions during the interglacial periods**

748

749 We focused on three interglacial periods: (i) MIS 31 and MIS 19 - because they
750 are potential analogues to Holocene in terms of orbital parameters - and (ii) MIS 21 -
751 because it is pivotal in the MPT, occurring just after glacial MIS22. Interestingly, the
752 deglaciation episodes leading to these three interglacials present strong differences.
753 Termination XV (MIS 32-31) is characterised by an abrupt decrease of benthic
754 foraminifer $\delta^{18}\text{O}_{\text{c}}$, while the two others (terminations X-MIS22/21 and IX - MIS20/19)
755 are more gradual (Figure 6). Furthermore, the beginning of the transitions to MIS 31 and
756 the MIS 21 show relatively cold sub-surface water conditions, while the sub-surface
757 water at MIS 20/19 transition is warmer (Figure 6).

758 As seen above, our data suggest that $\Delta 47$ -derived sub-surface temperatures
759 remained surprisingly cold during most of MIS31 (around 7-8°C), similar to glacial
760 temperatures, and only increased during the optimum of MIS31. We have no analytical
761 reason to reject these values, yet they provide very puzzling pieces of information about
762 sub-surface conditions during MIS31. Combining these low temperatures with the
763 corresponding $\delta^{18}\text{O}_{\text{c}}$ values result in seawater $\delta^{18}\text{O}_{\text{c}}$ that are much lower in the lower
764 part of MIS31 (i.e. $1.0\text{‰} \pm 0.6\text{‰}$ and $0.7\text{‰} \pm 0.6\text{‰}$ at 2SE, respectively) than any of the
765 other intervals studied in MJS. The subsurface $\delta^{18}\text{O}_{\text{sw}}$ at the beginning of MIS 31 are low
766 ($1.0\text{‰} \pm 0.6\text{‰}$ and $0.7\text{‰} \pm 0.6\text{‰}$ at 2SE). Such values could be attributed to a
767 combination of global signal (decrease of ice-sheet volume) and regional processes
768 (enhancement of runoff around the Mediterranean Sea and/or incursion of North

769 Atlantic water; Figure 6). Enhancement of runoff is supported by micropaleontological
770 and sedimentary data, which suggest a strong input of freshwater and the increase of
771 the detrital component from land, evidenced respectively by a peak in the high relative
772 abundance *Braarudosphaera bigelowii*, a low-salinity nannofossil species, and high Pl/Qz
773 ratios (Figure 7; Girone et al., 2013).

774 During MIS19, strong vertical stratification is associated to the deposition of a
775 sapropel-like event (Nomade et al., 2019). No sapropel-like layer has been found at MJS
776 during MIS 31, whereas in the Mediterranean Sea, the sapropel i-100 was deposited
777 during this interval. Further studies will be necessary to decipher whether specific
778 conditions blocked the deposition of a carbon-rich material in the Southern Apennines
779 foredeep during MIS 31.

780 The MIS 22/21 transition has been poorly documented at MJS in previous studies
781 and we cannot confront our data with other indicators. The MIS 20/19 transition, on the
782 opposite, has been extensively studied. Previous works have shown that the deglaciation
783 was characterized by several noticeable events: 1) the incursion of cold waters from the
784 North Atlantic resulting a thermic evolution typical of a *Heinrich-like* episode, with
785 moderately cold SST (PC1 nannofossils and foraminifera, abundance of *N. pachyderma*
786 left coiling in Figure 8), followed by a sharp interval of low SSTs (Maiorano et al., 2016),
787 and 2) the deposition of a sapropel-like event (Maiorano et al., 2016), corresponding to a
788 strong stratification of the water column (high $\Delta^{18}\text{O}_{c(p vs b)}$, and low $\delta^{13}\text{C}_{\text{benthic}}$ from
789 Nomade et al., 2019). Another possible source of freshwater could be sub-surface waters
790 from Adriatic origin that could gain their low $\delta^{18}\text{O}_{\text{sw}}$ signature from the melting of
791 Alpine glaciers.

792 Our data indicate that the climatic optimum occurred at the end of both MIS 31
793 and MIS 21, whereas it occurred at the beginning of the interglacial interval for MIS 19.
794 The MIS 31 covers two precession-cycles, the climate optimum being associated with
795 the second precession-related peak of summer insolation (Figure 2). This climatic
796 optimum shows a sub-surface temperature of $13.8\text{ }^{\circ}\text{C} \pm 3\text{ }^{\circ}\text{C}$ (2SE), whereas it is $14.8 \pm$
797 $2.6\text{ }^{\circ}\text{C}$ (2SE) for MIS19. Among the three interglacials studied, MIS 21 shows the highest
798 sub-surface temperature: $16.6\text{ }^{\circ}\text{C} \pm 3\text{ }^{\circ}\text{C}$ (2SE). All interglacial periods following MIS 19,
799 also show their climatic optimum associated to the first strong precession-related
800 summer insolation peak. Furthermore, we observed increase in $\delta^{18}\text{O}_{\text{sw}}$ during the
801 climate optimum of MIS 31, with similar values to those recorded at the climatic

802 optimum for interglacials MIS 21 and MIS 19. It is worth to notice that these $\delta^{18}\text{O}_{\text{sw}}$
803 reconstructions are also similar, within the limits of our error bars, to the glacial $\delta^{18}\text{O}_{\text{sw}}$
804 baseline (Figure 6).

805 The current, annually-averaged temperatures in the Gulf of Taranto are $\sim 23\text{-}24$
806 $^{\circ}\text{C}$ at the surface and ~ 14 $^{\circ}\text{C}$ at 300 m depth (Figure 3; Pinardi et al., 2016). Thus,
807 temperatures recorded at the climatic optimums are comparable to modern conditions
808 below the thermocline in the Gulf of Taranto. Furthermore, the current $\delta^{18}\text{O}_{\text{sw}}$ at 500 m
809 depth is ~ 1.7 ‰, which is also similar to the reconstructed $\delta^{18}\text{O}_{\text{sw}}$ for MIS 31 and MIS
810 19. Interestingly, the reconstructed sub-surface temperature and $\delta^{18}\text{O}_{\text{sw}}$ during MIS 21
811 are was higher than the Holocene values.

812

813

814 7. Conclusions

815

816 By combining clumped-isotope temperature reconstructions with higher-
817 temporal resolution proxies, we document paleoenvironmental changes over five glacial
818 periods (MIS 36, 34, 30, 22 and 20) and three interglacials (MIS 31, 21 and 19)
819 throughout the Mid-Pleistocene series exposed at Montalbano Ionico (Southern Italy),
820 along the Gulf of Taranto. Over a few intervals, our data revealed large discrepancies
821 between Mg/Ca and Δ_{47} -derived temperatures. These observations suggest that Mg/Ca-
822 paleotemperature data may be biased, although one cannot provide any conclusive
823 explanation about the mechanisms at play. In this work, we favoured the clumped-
824 isotope thermometer data to reconstruct benthic (sub-surface) past seawater
825 paleotemperatures.

826 During the climatic optimums of MIS 31 and MIS 19, considered as close
827 analogues to the current interglacial in terms of insolation forcing, reconstructed sub-
828 surface temperatures from benthic foraminifer analyses ($13.8 \pm 1.5^{\circ}\text{C}$ and $14.8 \pm 1.3^{\circ}\text{C}$,
829 respectively) and $\delta^{18}\text{O}_{\text{sw}}$ are similar to the ones measured today below the thermocline
830 in the Gulf of Taranto.

831 Our results show that temperature conditions were similar in all the studied
832 glacial periods across the MPT suggesting that oceanographic conditions in the
833 Mediterranean Sea were relatively stable between the 41 ka-world and the 100 ka-
834 world or that the tectonic uplift that took place at MJS during this transition balanced
835 out the MPT cooling trend through the shallowing of the deposition site.

836

837

838 **Acknowledgment**

839

840 We gratefully thank the two anonymous reviewers for their recommendations that
841 significantly improved the final manuscript. MP thanks G. Siani, N. Meckler, C. John, B.
842 Malaize, T. De Garidel-Thoron and the Paleocean team from LSCE for the fruitful
843 discussions, and A. Pereira and V. Scao for their invaluable help in the field. MP received
844 a PhD fellowship from CEA (Commissariat a l'Energie Atomique et aux Energies
845 Alternatives, France). All the isotopic and trace-element analyses have been performed
846 on IRMS and ICP-MS belonging to the Analytical Platform PANOPLY (LSCE-GEOPS). The
847 Mg/Ca measurements were financially supported by the LEFE/MAGICS project.

848

849 **References**

850

- 851 Aiello G., Barra D. and Parisi R. (2015) Lower-Middle Pleistocene ostracod assemblages
852 from the Montalbano Jonico section (Basilicata, Southern Italy). *Quat. Int.* **383**, 47–
853 73. Available at: <http://dx.doi.org/10.1016/j.quaint.2014.11.010>.
- 854 Alpert, P., Baldi, M., Ilani, R., Krichak, S., Price, C., Rodo, X., ... & Mariotti, A. (2006).
855 Relations between climate variability in the Mediterranean region and the tropics:
856 ENSO, South Asian and African monsoons, hurricanes and Saharan dust.
857 *Developments in Earth and Environmental Sciences.* **4**, 149-177.
- 858 Altenbach A. V., Pflaumann U., Schiebel R., Thies A., Timm S. and Trauth M. (1999)
859 Scaling percentages and distributional patterns of benthic Foraminifera with flux
860 rates of organic carbon. *J. Foraminifer. Res.* **29**, 173–185. Available at:
861 <http://jfr.geoscienceworld.org/content/29/3/173.abstract>.
- 862 Anand P., Elderfield H. and Conte M. H. (2003) Calibration of Mg / Ca thermometry in
863 planktonic foraminifera from a sediment trap time series. **18**.
- 864 Arbuszewski, J., P. Demenocal, A. Kaplan, and E. C. Farmer (2010), On the fidelity of
865 shell-derived d18O seawater estimates, *Earth Planet. Sci. Lett.*, 300, 185–196,
866 doi:10.1016/j. epsl.2010.10.035.
- 867 Balduzzi A., Casnedi R., Crescenti U., Mostardini F. and Tonna M. (1982) Il Plio-
868 Pleistocene del sottosuolo del bacino lucano (Avanfossa appenninica). *Geol. Rom.* **21**,
869 89–111.
- 870 Barker S., Greaves M. and Elderfield H. (2003) A study of cleaning procedures used for
871 foraminiferal Mg/Ca paleothermometry. *Geochemistry, Geophys. Geosystems* **4**, 1–20.
- 872 Bernasconi S. M., Müller I. A., Bergmann K. D. and Sebastian F. M. Reducing uncertainties
873 in carbonate clumped isotope analysis through consistent carbonate - based
874 standardization.
- 875 Bertini A., Toti F., Marino M. and Ciaranfi N. (2015) Vegetation and climate across the
876 Early-Middle Pleistocene transition at Montalbano Jonico, southern Italy. *Quat. Int.*
877 **383**, 74–88.
- 878 Bignami, F., Sciarra, R., Carniel, S., and Santoleri, R. (2007) Variability of Adriatic Sea

879 coastal turbid waters from SeaWiFS imagery. *Journal of Geophysical Research* **112**,
880 C03S10.

881 Bintanja R. and Van De Wal R. S. W. (2008) North American ice-sheet dynamics and the
882 onset of 100,000-year glacial cycles. *Nature* **454**, 869–872.

883 Bintanja R., Van De Wal R. S. W. and Oerlemans J. (2005) Modelled atmospheric
884 temperatures and global sea levels over the past million years. *Nature* **437**, 125–
885 128.

886 Boussetta S., Bassinot F., Sabbatini A., Caillon N., Nouet J., Kallel N., Rebaubier H.,
887 Klinkhammer G. and Labeyrie L. (2011) Diagenetic Mg-rich calcite in Mediterranean
888 sediments: Quantification and impact on foraminiferal Mg/Ca thermometry. *Mar.*
889 *Geol.* **280**, 195–204. Available at: <http://dx.doi.org/10.1016/j.margeo.2010.12.011>.

890 Brand W. A., Assonov S. S. and Coplen T. B. (2010) Correction for the 17O interference in
891 $\delta(13C)$ measurements when analyzing CO₂ with stable isotope mass spectrometry
892 (IUPAC Technical Report). *Pure Appl. Chem.* **82**, 1719–1733. Available at:
893 [https://www.degruyter.com/view/j/pac.2010.82.issue-8/pac-rep-09-01-05/pac-](https://www.degruyter.com/view/j/pac.2010.82.issue-8/pac-rep-09-01-05/pac-rep-09-01-05.xml)
894 [rep-09-01-05.xml](https://www.degruyter.com/view/j/pac.2010.82.issue-8/pac-rep-09-01-05/pac-rep-09-01-05.xml).

895 Brandimarte, L., Di Baldassarre, G., Bruni, G., D'Odorico, P. and Montanari, A. (2011)
896 Relation between the North-Atlantic Oscillation and hydroclimatic conditions in
897 Mediterranean areas. *Water Resources Management* **25** (5), 1269–79.

898 Brilli, M., 1998. Stratigrafia isotopica del carbonio e dell'ossigeno della successione infra
899 e mesopliocenica di Montalbano Jonico (Basilicata, Italia meridionale). Tesi di
900 Dottorato di Ricerca in Scienze della terra XI ciclo. Università degli Studi di Roma
901 "La Sapienza" 112 pp

902 Brilli M., Lerche L., Ciaranfi N. and Turi B. (2000) Evidences of precession and obliquity
903 orbital forcing in oxygen-18 isotope composition of Montalbano Jonico Section
904 (Basilicata, southern Italy). *Appl. Radiat. Isot.* **52**, 957–964.

905 Broecker, W., and T. H. Peng, Tracers in the Sea, 690 pp., Eldigio, Palisades, N.Y., 1982

906 Bruland, K. W. (1983). Trace elements in seawater.

907 Casnedi R. (1988) La Fossa bradanica: origine, sedimentazione e migrazione. *Mem. Soc.*
908 *Geol. It* **41**, 439–448.

909 Casnedi R., Crescenti U. and Tonna M. (1982) Evoluzione dell'avanfossa adriatica
910 meridionale nel Plio-Pleistocene, sulla base di dati di sottosuolo. *Mem. Soc. Geol. It*
911 **24**, 243–260.

912 Català, A., Cacho, I., Frigola, J., Pena, L. D., & Lirer, F. (2019). Holocene hydrography
913 evolution in the Alboran Sea: a multi-record and multi-proxy comparison. *Climate of*
914 *the Past*, **15**(3), 927-942.

915 Cessi, P., Pinardi, N., and Lyubartsev, V. (2014) Energetics of Semienclosed Basins with
916 Two-Layer Flows at the Strait, *J. Phys. Oceanogr.* **44**, 967–979, doi:10.1175/JPO-D-
917 13-0129.1

918 Chalk T. B., Hain M. P., Foster G. L., Rohling E. J., Sexton P. F. and Badger M. P. S. (2017)
919 Causes of ice age intensification across the Mid-Pleistocene Transition. *Pnas* **114**,
920 13114–13119.

921 Ciaranfi N., Lirer F., Lirer L., Lourens L. J., Maiorano P., Marino M., Petrosino P., Sprovieri
922 M., Stefanelli S., Brilli M., Girone A., Joannin S., Pelosi N. and Vallefucio M. (2010)
923 Integrated stratigraphy and astronomical tuning of lower-middle Pleistocene
924 Montalbano Jonico section (southern Italy). *Quat. Int.* **219**, 109–120. Available at:
925 <http://dx.doi.org/10.1016/j.quaint.2009.10.027>.

926 Cisneros, M., Cacho, I., Frigola, J., Canals, M., Martrat, B., Casado, M., ... & Lirer, F. (2016).
927 Sea surface temperature variability in the central-western Mediterranean Sea

928 during the last 2700 years: a multi-proxy and multi-record approach.

929 Civitarese, G., Gačić, M., Lipizer, M., & Eusebi Borzelli, G. L. (2010). On the impact of the

930 Bimodal Oscillating System (BiOS) on the biogeochemistry and biology of the

931 Adriatic and Ionian Seas (Eastern Mediterranean). *Biogeosciences*, 7(12), 3987-

932 3997.

933 Coletti A. J., DeConto R. M., Brigham-Grette J. and Melles M. (2015) A GCM comparison of

934 Pleistocene super-interglacial periods in relation to Lake El'gygytyn, NE Arctic

935 Russia. *Clim. Past* **11**, 979–989.

936 Daëron M., Blamart D., Peral M. and Affek H. (2016) Absolute isotopic abundance ratios

937 and the accuracy of $\Delta 47$ measurements. , 1–39.

938 D'Alessandro A., La Perna R. and Ciaranfi N. (2003) Response of macrobenthos to

939 changes in palaeoenvironments in the Lower–Middle Pleistocene (Lucania Basin,

940 Southern Italy). *Quat.* **16**, 167–183.

941 Deconto R. M., Galeotti S., Pagani M., Tracy D., Schaefer K., Zhang T., Pollard D. and

942 Beerling D. J. (2012) carbon release from thawing permafrost. , 6–11.

943 Eiler, J.M. (2007) “Clumped-isotope” geochemistry-the study of naturally-occurring,

944 multiply-substituted isotopologues. *Earth Planet. Sci. Lett.* **262**, 309–327.

945 Eiler, J.M. (2011) Paleoclimate reconstruction using carbonate clumped isotope

946 thermometry. *Quat. Sci. Rev.* **30** (25–26), 3575–3588. [https://doi.org/10.1016/j.](https://doi.org/10.1016/j.quascirev.2011.09.001)

947 [quascirev.2011.09.001](https://doi.org/10.1016/j.quascirev.2011.09.001)

948 Elderfield H., Greaves M., Barker S., Hall I. R., Tripathi A., Ferretti P., Crowhurst S., Booth L.

949 and Daunt C. (2010) A record of bottom water temperature and seawater $\delta 18 O$ for

950 the Southern Ocean over the past 440 kyr based on Mg / Ca of benthic foraminiferal

951 *Uvigerina* spp. *Quat. Sci. Rev.* **29**, 160–169. Available at:

952 <http://dx.doi.org/10.1016/j.quascirev.2009.07.013>.

953 Elderfield H., Yu J., Anand P., Kiefer T. and Nyland B. (2006) Calibrations for benthic

954 foraminiferal Mg/Ca paleothermometry and the carbonate ion hypothesis. *Earth*

955 *Planet. Sci. Lett.* **250**, 633–649.

956 Emeis K., Struck U., Schulz H., Rosenberg R., Bernasconi S., Erlenkeuser H., Sakamoto T.

957 and Martinez-ruiz F. (2000) Temperature and salinity variations of Mediterranean

958 Sea surface waters over the last 16, 000 years from records of planktonic stable

959 oxygen isotopes and alkenone unsaturation ratios. **158**, 259–280.

960 Ferguson, J., G. Henderson, M. Kucera, and R. Rickaby (2008), Systematic change of

961 foraminiferal Mg/Ca ratios across a strong salinity gradient, *Earth Planet. Sci. Lett.*,

962 265, 153–166, doi:10.1016/j.epsl.2007.10.011.

963 Fontanier C., Jorissen F. J., Licari L., Alexandre A., Anschutz P. and Carbonel P. (2002)

964 Live benthic foraminiferal faunas from the Bay of Biscay: Faunal density,

965 composition, and microhabitats. *Deep. Res. Part I Oceanogr. Res. Pap.* **49**, 751–785.

966 Giaccio B., Regattieri E., Zanchetta G., Nomade S., Renne P. R., Sprain C. J., Drysdale R. N.,

967 Tzedakis P. C., Messina P., Scardia G., Sposato A. and Bassinot F. (2015) Duration and

968 dynamics of the best orbital analogue to the present interglacial. *Geology* **43**, 603–

969 606.

970 Giorgi, F. (2006) Regional climate modeling: status and perspectives. *J. Phys.* **IV 139**,

971 101–118. <http://dx.doi.org/10.1051/jp4:2006139008>.

972 Girone A., Capotondi L., Ciaranfi N., Di Leo P., Lirer F., Maiorano P., Marino M., Pelosi N.

973 and Pulice I. (2013) Paleoenvironmental changes at the lower Pleistocene

974 Montalbano Jonico section (southern Italy): Global versus regional signals.

975 *Palaeogeogr. Palaeoclimatol. Palaeoecol.* **371**, 62–79. Available at:

976 <http://dx.doi.org/10.1016/j.palaeo.2012.12.017>.

- 977 Ghosh, P., Adkins, J., Affek, H., Balta, B., Guo, W., Schauble, E.A., Schrag, D., Eiler, J.M.
 978 (2006) 13C–18O bonds in carbonate minerals: a new kind of paleothermometer.
 979 *Geochim. Cosmochim. Acta* **70** (6), 1439–1456. [https://doi.org/10.1016/j.gca.2005.](https://doi.org/10.1016/j.gca.2005.11.014)
 980 11.014.
- 981 Goudeau M.L.S., Grauel, A.L., Tessarolo, C., Leider, A., Chen, L., Bernasconi,
 982 S.M., Versteegh, G.J.M., Zonneveld, K.A.F., Boer, W., Alonso-Hernandez, C.M., De
 983 Lange, G.J. (2014). The Glacial-interglacial transition and Holocene environmental
 984 changes in sediments from the Gulf of Taranto, central Mediterranean. *Mar.*
 985 *Geol.* **348**, 88-102
- 986 Goyet, C., Healy, R., Ryan, J., & Kozyr, A. (2000). *Global distribution of total inorganic*
 987 *carbon and total alkalinity below the deepest winter mixed layer depths* (No.
 988 ORNL/CDIAC-127; NDP-076). Oak Ridge National Lab., TN (US).
- 989 Grauel A. L., Schmid T. W., Hu B., Bergami C., Capotondi L., Zhou L. and Bernasconi S. M.
 990 (2013) Calibration and application of the “clumped isotope” thermometer to
 991 foraminifera for high-resolution climate reconstructions. *Geochim. Cosmochim. Acta*
 992 **108**, 125–140. Available at: <http://dx.doi.org/10.1016/j.gca.2012.12.049>.
- 993 Gray, W. R., Weldeab, S., Lea, D. W., Rosenthal, Y., Gruber, N., Donner, B., & Fischer, G.
 994 (2018). The effects of temperature, salinity, and the carbonate system on Mg/Ca in
 995 Globigerinoides ruber (white): A global sediment trap calibration. *Earth and*
 996 *Planetary Science Letters*, **482**, 607–620.
 997 <https://doi.org/10.1016/j.epsl.2017.11.026>
- 998 Grossman E. L. (1987) Stable isotopes in modern benthic foraminifera; a study of vital
 999 effect. *J. Foraminifer. Res.* **17**, 48–61.
- 1000 Guarnieri, A., Pinardi, N., Oddo, P., Bortoluzzi, G., and Ravaioli, M. (2013) Impact of tides
 1001 in a baroclinic circulation model of the Adriatic Sea, *J. Geophys. Res.-Oceans*, **118**,
 1002 166–183, doi:10.1029/2012jc007921
- 1003 Head M. J. and Gibbard P. L. (2015) Early-Middle Pleistocene transitions: Linking
 1004 terrestrial and marine realms. *Quat. Int.* **389**, 7–46. Available at:
 1005 <http://dx.doi.org/10.1016/j.quaint.2015.09.042>.
- 1006 Helmke J. P., Bauch H. A. and Erlenkeuser H. (2003) Development of glacial and
 1007 interglacial conditions in the Nordic seas between 1.5 and 0.35 Ma. *Quat. Sci. Rev.*
 1008 **22**, 1717–1728.
- 1009 Hillaire-Marcel C., De Vernal A. and McKay J. (2011) Foraminifer isotope study of the
 1010 Pleistocene Labrador Sea, northwest North Atlantic (IODP Sites 1302/03 and 1305),
 1011 with emphasis on paleoceanographical differences between its “inner” and “outer”
 1012 basins. *Mar. Geol.* **279**, 188–198.
- 1013 Hönisch B., Hemming N. G., Archer D., Siddall M. and McManus J. F. (2009) Atmospheric
 1014 carbon dioxide concentration across the mid-Pleistocene transition. *Science* **324**,
 1015 1551–4. Available at:
 1016 <http://www.sciencemag.org/cgi/doi/10.1126/science.1171477>
 1017 <http://www.ncbi.nlm.nih.gov/pubmed/19541994>.
- 1018 Hurrell, J. W. (1995) Decadal trends in the north Atlantic oscillation: Regional
 1019 temperatures and precipitation. *Science* **269** (5224), 676-679.
- 1020 Joannin S., Ciaranfi N. and Stefanelli S. (2008) Vegetation changes during the late Early
 1021 Pleistocene at Montalbano Jonico (Province of Matera, southern Italy) based on
 1022 pollen analysis. *Palaeogeogr. Palaeoclimatol. Palaeoecol.* **270**, 92–101.
- 1023 Kim S.-T. and O’Neil J. R. (1997) Equilibrium and nonequilibrium oxygen isotope effects
 1024 in synthetic carbonates. *Geochim. Cosmochim. Acta* **61**, 3461–3475. Available at:
 1025 <http://linkinghub.elsevier.com/retrieve/pii/S0016703797001695>.

1026 Kisakürek, B., A. Eisenhauer, F. Böhm, D. Garbe-Schönberg, and J. Erez (2008), Controls
1027 on shell Mg/Ca and Sr/Ca in cultured planktonic foraminiferan, *Globigerinoides*
1028 *ruber* (white), *Earth Planet. Sci. Lett.*, **273**, 260–269, doi:10.1016/
1029 *j.epsl.2008.06.026*.

1030 Konijnendijk T. Y. M., Ziegler M. and Lourens L. J. (2014) Chronological constraints on
1031 Pleistocene sapropel depositions from high-resolution geochemical records of ODP
1032 Sites 967 and 968. *Newsletters Stratigr.* **47**, 263–282. Available at:
1033 [http://openurl.ingenta.com/content/xref?genre=article&issn=0078-](http://openurl.ingenta.com/content/xref?genre=article&issn=0078-0421&volume=47&issue=3&spage=263)
1034 [0421&volume=47&issue=3&spage=263](http://openurl.ingenta.com/content/xref?genre=article&issn=0078-0421&volume=47&issue=3&spage=263).

1035 Lea, D., T. Mashiotta, and H. Spero (1999), Controls on magnesium and strontium uptake
1036 in planktonic foraminifera determined by live culturing, *Geochim. Cosmochim. Acta*,
1037 **63**, 2369–2379, doi:10.1016/S0016-7037(99)00197-0.

1038 Lang N. and Wolff E. W. (2011) of the Past Interglacial and glacial variability from the
1039 last 800 ka in marine , ice and terrestrial archives. , 361–380.

1040 Laskar J., Robutel P., Joutel F., Gastineau M., Correia A. C. M. and Levrard B. (2004)
1041 Astrophysics A long-term numerical solution for the insolation. **285**, 261–285.

1042 Lionello, P., Malanotte-Rizzoli, P., Boscolo, R., Alpert, P., Artale, V., Li, L., Luterbacher J.,
1043 May W., Trigo R., Tsimplis M., Ulbrich U., Xoplaki E. (2006). The Mediterranean
1044 climate: an overview of the main characteristics and issues. *Dev. Earth Environ. Sci.*
1045 **4** (C), 1–26.

1046 Lisiecki L. E. and Raymo M. E. (2005) A Pliocene-Pleistocene stack of 57 globally
1047 distributed benthic $\delta^{18}O$ records. **20**, 1–17.

1048 Lourens L. J. (2004) Revised tuning of Ocean Drilling Program Site 964 and KC01B (
1049 Mediterranean) and implications for the $\delta^{18}O$, tephra , calcareous nannofossil ,
1050 and geomagnetic reversal chronologies of the past 1 . 1 Myr. **19**, 1–20.

1051 Maiorano P., Marino M., di Stefano E. and Ciaranfi N. (2004) Calcareous nannofossil
1052 events in the Lower-Middle Pleistocene transition at the Montalbano Jonico section
1053 and ODP site 964: Calibration with isotope and sapropel stratigraphy. *Riv. Ital. di*
1054 *Paleontol. e Stratigr.* **110**, 547–557.


1055 Maiorano P., Capotondi L., Ciaranfi N., Girone a, Lirer F., Marino M., Pelosi N., Petrosino
1056 P. and Piscitelli a (2010) Vrica-Crotone and Montalbano Jonico sections: A potential
1057 unit-stratotype of the Calabrian Stage. *Episodes* **33**, 218–233. Available at:
1058 [http://www.scopus.com/inward/record.url?eid=2-s2.0-](http://www.scopus.com/inward/record.url?eid=2-s2.0-79957631816&partnerID=40&md5=9cd1dec5a710f096255da80208d8f766)
1059 [79957631816&partnerID=40&md5=9cd1dec5a710f096255da80208d8f766](http://www.scopus.com/inward/record.url?eid=2-s2.0-79957631816&partnerID=40&md5=9cd1dec5a710f096255da80208d8f766).

1060 Maiorano P., Bertini A., Capolongo D., Eramo G., Gallicchio S., Girone A., Pinto D., Toti F.,
1061 Ventruti G. and Marino M. (2016) Climate signatures through Marine Isotope Stage
1062 19 in the Montalbano Jonico section (Southern Italy): A land–sea perspective.
1063 *Palaeogeogr. Palaeoclimatol. Palaeoecol.* **461**, 341–361. Available at:
1064 <http://linkinghub.elsevier.com/retrieve/pii/S0031018216303819>.

1065 Marino M., Bertini A., Ciaranfi N., Aiello G., Barra D., Gallicchio S., Girone A., La Perna R.,
1066 Lirer F., Maiorano P., Petrosino P. and Toti F. (2015) Paleoenvironmental and
1067 climatostratigraphic insights for Marine Isotope Stage 19 (Pleistocene) at the
1068 Montalbano Jonico succession, South Italy. *Quat. Int.* **383**, 104–115.

1069 Mathien-Blard E. and Bassinot F. (2009) Salinity bias on the foraminifera Mg/Ca
1070 thermometry: Correction procedure and implications for past ocean hydrographic
1071 reconstructions. *Geochemistry, Geophys. Geosystems* **10**.

1072 Mcclymont E. L., Rosell-mele A., Haug G. H. and Lloyd J. M. (2008) Expansion of subarctic
1073 water masses in the North Atlantic and Pacific oceans and implications for mid-
1074 Pleistocene ice sheet growth. **23**, 1–12.

- 1075 Meckler A. N., Ziegler M., Mill??n M. I., Breitenbach S. F. M. and Bernasconi S. M. (2014)
 1076 Long-term performance of the Kiel carbonate device with a new correction scheme
 1077 for clumped isotope measurements. *Rapid Commun. Mass Spectrom.* **28**, 1705–1715.
- 1078 Melles M., Melles M., Brigham-grette J., Minyuk P. S., Nowaczyk N. R., Wennrich V.,
 1079 Deconto R. M., Anderson P. M., Andreev A. A., Coletti A., Cook T. L., Haltia-hovi E.,
 1080 Kukkonen M., Lozhkin A. V, Rosén P., Tarasov P., Vogel H. and Wagner B. (2014) 2 . 8
 1081 Million Years of Arctic Climate. *Science (80-)*. **315**.
- 1082 Milligan, T.G., Cattaneo, A. (2007) Sediment dynamics in the western Adriatic Sea: from
 1083 transport to stratigraphy. *Cont. Shelf Res.* **27**, 287–295.
- 1084 Murray J. W. (1963) Ecological exeriments on Foraminiferida. *J. Mar. Biol. Assoc. United*
 1085 *Kingdom* **43**, 621–642.
- 1086 Murray J. (2006) *Ecology and Applications of Benthic Foraminifera*. ed. Cambridge
 1087 university press, United States of America by Cambridge University Press, new York.
- 1088 Naafs B. D. A., Hefter J. and Stein R. (2013) Millennial-scale ice rafting events and Hudson
 1089 Strait Heinrich (-like) Events during the late Pliocene and Pleistocene: a review.
 1090 *Quat. Sci. Rev.* **80**, 1–28.
- 1091 Nomade S., Bassinot F., Marino M., Simon Q., Dewilde F., Maiorano P., Isguder G., Blamart
 1092 D., Girone A., Scao V., Pereira A., Toti F., Bertini A., Combourieu-Nebout N., Peral M.,
 1093 Boulès D. L., Petrosino P., Gallicchio S. and Ciaranfi N. (2019) High-resolution
 1094 foraminifer stable isotope record of MIS 19 at Montalbano Jonico, southern Italy: A
 1095 window into Mediterranean climatic variability during a low-eccentricity
 1096 interglacial. *Quat. Sci. Rev.* **205**, 106–125.
- 1097 Nürnberg, D., J. Bijma, and C. Hemleben (1996), Assessing the reliability of magnesium
 1098 in foraminiferal calcite as a proxy for water mass temperatures, *Geochim.*
 1099 *Cosmochim. Acta*, **60**, 803–814, doi:10.1016/0016-7037(95)00446-7.
- 1100 Oliveira D., S M. F., Naughton F., Polanco-martínez J. M., Jimenez-espejo F. J., Grimalt J. O.,
 1101 Martrat B., Voelker A. H. L., Trigo R., Hodell D. A., Abrantes F. and Desprat S. (2017)
 1102 Unexpected weak seasonal climate in the western Mediterranean region during MIS
 1103 31 , a high-insolation forced interglacial nchez Go n. *Quat. Sci. Rev.* **161**, 1–17.
- 1104 Patacca, E., Scandone, P., 2004. The Plio-Pleistocene thrust belt-foredeep system in the
 1105 southern Apennines and Sicily (Italy). In: *Crescenti, et al. (Ed.), Special Volume of the*
 1106 *Italian Geological Society for the IGC 32 Florence 2004. Società Geologica Italiana,*
 1107 *Roma*, pp. 93–129. 
- 1108 Peral M., Daëron M., Blamart D., Bassinot F., Dewilde F., Smialkowski N., Isguder G.,
 1109 Jorissen F., Kissel C., Michel E., Va N. and Waelbroeck C. (2018) ScienceDirect
 1110 Updated calibration of the clumped isotope thermometer in planktonic and benthic
 1111 foraminifera. **239**, 1–16.
- 1112 Petrosino P., Jicha B. R., Mazzeo F. C., Ciaranfi N., Girone A., Maiorano P. and Marino M.
 1113 (2015) The Montalbano Jonico marine succession: An archive for distal tephra
 1114 layers at the Early-Middle Pleistocene boundary in southern Italy. *Quat. Int.* **383**,
 1115 89–103.
- 1116 Piervitali, E., Colacino, M. and Conte. M. (1997) Signals of climatic change in the Central-
 1117 Western Mediterranean basin. *Theoretical and Applied Climatology.* **58** (3-4), 211-9.
- 1118 Pinardi N., Lyubartsev V., Cardellicchio N., Caporale C., Ciliberti S., Coppini G., Pascalis F.
 1119 De, DIALTI L., Federico I., Filippone M., Grandi A., Guideri M., Lecci R., Lamberti L.,
 1120 Lorenzetti G., Lusiani P., Macripo C. D., Maicu F., Mossa M., Tartarini D., Trotta F.,
 1121 Umgiesser G. and Zaggia L. (2016) Marine Rapid Environmental Assessment in the
 1122 Gulf of Taranto : a multiscale approach. , 2623–2639.
- 1123 Pol K., Masson-Delmotte V., Johnsen S., Bigler M., Cattani O., Durand G., Falourd S., Jouzel

1124 J., Minster B., Parrenin F., Ritz C., Steen-Larsen H. C. and Stenni B. (2010) New MIS
1125 19 EPICA Dome C high resolution deuterium data: Hints for a problematic
1126 preservation of climate variability at sub-millennial scale in the “oldest ice.” *Earth*
1127 *Planet. Sci. Lett.* **298**, 95–103. Available at:
1128 <http://dx.doi.org/10.1016/j.epsl.2010.07.030>.

1129 Pollard D. and DeConto R. M. (2009) Modelling West Antarctic ice sheet growth and
1130 collapse through the past five million years. *Nature* **458**, 329–332.

1131 Poulain, P-M. (2001) Adriatic Sea surface circulation as derived from drifter data
1132 between 1990 and 1999. *Journal of Marine Systems* **29** (1-4) (5), 3-32.

1133 Raitzsch M., Kuhnert H., Groeneveld J. and Bickert T. (2008) Benthic foraminifer Mg/Ca
1134 anomalies in South Atlantic core top sediments and their implications for
1135 paleothermometry. *Geochemistry, Geophys. Geosystems* **9**.

1136 Regattieri E., Giaccio B., Zanchetta G., Mannella G., Nomade S., Vogel H., Tognarelli A.,
1137 Boschi C., Perchiazzi N. and Galli P. (2018) Expression, frequencies and dynamics of
1138 sub-orbital scale variability during Marine Isotope Stages 19: insights from the
1139 Sulmona Basin (central Italy). In *EGU General Assembly Conference Abstracts* p.
1140 3464.

1141 Regattieri, E., Giaccio, B., Mannella, G., Zanchetta, G., Nomade, S., Tognarelli, A.,
1142 Perchiazzi, N., Vogel, H., Boschi, C., Neil, R. D., Wagner, B., Gemelli, M., Tzedakis, P.
1143 (2019) Frequency and dynamics of millennial-scale variability during Marine
1144 Isotope Stage 19: Insights from the Sulmona Basin (central Italy). *Quaternary*
1145 *Science Reviews* 214, 28-43

1146 Rossignol-Strick M. and Paterne M. (1999) A synthetic pollen record of the eastern
1147 Mediterranean sapropels of the last 1 Ma: implications for the time-scale and
1148 formation of sapropels. *Mar. Geol.* **153**, 221–237.

1149 Riley, J. P., & Skirrow, G. (1975). Appendix Table 6. *JP RILEY & G. SKIRROW. Chemical*
1150 *Oceanography*, 1, 561-562.

1151 Ruddiman W. F., Raymo M. and McIntyre A. (1986) Matuyama 41,000-year cycles: North
1152 Atlantic Ocean and northern hemisphere ice sheets. *Earth Planet. Sci. Lett.* **80**, 117–
1153 129.

1154 Ruddiman W. F., Sarnthein M., Backman J., Baldauf J. G., Curry W., Dupont L. M., Janecek
1155 T., Pokras E. M., Raymo M. E., Stabell B., Stein R. and Tiedemann R. (1989) Late
1156 Miocene to Pleistocene Evolution of Climate in Africa and the Low-Latitude Atlantic:
1157 Overview of Leg 108 Results. *Proc. Ocean Drill. Program, 108 Sci. Results* **108**, 463–
1158 484. Available at: [http://www-](http://www-odp.tamu.edu/publications/108_SR/VOLUME/CHAPTERS/sr108_29.pdf)
1159 [odp.tamu.edu/publications/108_SR/VOLUME/CHAPTERS/sr108_29.pdf](http://www-odp.tamu.edu/publications/108_SR/VOLUME/CHAPTERS/sr108_29.pdf).

1160 Russell, A. D., B. Hönisch, H. J. Spero, and D. W. Lea (2004), Effects of seawater carbonate
1161 ion concentration and temperature on shell U, Mg, and Sr in cultured planktonic
1162 foraminifera, *Geochim. Cosmochim. Acta*, 68(21), 4347–4361,
1163 doi:10.1016/j.gca.2004.03.013

1164 Sabbatini A., Bassinot F., Boussetta S., Negri A., Rebaubier H., Dewilde F., Nouet J., Caillon
1165 N. and Morigi C. (2011) Further constraints on the diagenetic influences and salinity
1166 effect on Globigerinoides ruber (white) Mg/Ca thermometry: Implications in the
1167 Mediterranean Sea. *Geochemistry, Geophys. Geosystems* **12**.

1168 Sánchez-Goñi M. F., Llave E., Oliveira D., Naughton F., Desprat S. and Ducassou E. (2016)
1169 Climate changes in south western Iberia and Mediterranean Out flow variations
1170 during two contrasting cycles of the last 1 Myrs : MIS 31 – MIS. *Glob. Planet. Change*
1171 **136**, 18–29. Available at: <http://dx.doi.org/10.1016/j.gloplacha.2015.11.006>.

1172 Savini, A., & Corselli, C. (2010). High-resolution bathymetry and acoustic geophysical

- 1173 data from Santa Maria di Leuca Cold Water Coral province (Northern Ionian Sea—
 1174 Apulian continental slope). *Deep Sea Research Part II: Topical Studies in*
 1175 *Oceanography*, 57(5-6), 326-344.
- 1176 Schauble E. A., Ghosh P. and Eiler J. M. (2006) Preferential formation of ^{13}C - ^{18}O bonds
 1177 in carbonate minerals, estimated using first-principles lattice dynamics. *Geochim.*
 1178 *Cosmochim. Acta* **70**, 2510–2529.
- 1179 Scherer R. P., Bohaty S. M., Dunbar R. B., Esper O., Flores J. A., Gersonde R., Harwood D.
 1180 M., Roberts A. P. and Taviani M. (2008) Antarctic records of precession-paced
 1181 insolation-driven warming during early Pleistocene Marine Isotope Stage 31.
 1182 *Geophys. Res. Lett.* **35**, 1–5.
- 1183 Sellschopp, J. and Álvarez, A. (2003) Dense low-salinity outflow from the Adriatic sea
 1184 under mild (2001) and strong (1999) winter conditions. *Journal of Geophysical*
 1185 *Research*. **108** (C9), 8104
- 1186 Simon Q., Bourlès D. L., Bassinot F., Nomade S., Marino M., Ciaranfi N., Girone A.,
 1187 Maiorano P., Thouveny N., Choy S., Dewilde F., Scao V., Isguder G., Blamart D. and
 1188 Team A. (2017) Authigenic ^{10}Be / ^9Be ratio signature of the Matuyama – Brunhes
 1189 boundary in the Montalbano Jonico marine succession. *Earth Planet. Sci. Lett.* **460**,
 1190 255–267. Available at: <http://dx.doi.org/10.1016/j.epsl.2016.11.052>.
- 1191 Stefanelli S. (2003) Benthic foraminiferal assemblages as tools for paleoenvironmental
 1192 reconstruction of the early-middle Pleistocene Montalbano Jonico composite
 1193 section. *BOLLETTINO-SOCIETA Paleontol. Ital.* **42**, 281–300.
- 1194 Stefanelli S., Capotondi L. and Ciaranfi N. (2005) Foraminiferal record and
 1195 environmental changes during the deposition of the Early-Middle Pleistocene
 1196 sapropels in southern Italy. *Palaeogeogr. Palaeoclimatol. Palaeoecol.* **216**, 27–52.
- 1197 Theocharis A., and Georgopoulos D. (1993) Dense water formation over the Samothraki
 1198 and Limnos Plateaux in the north Aegean Sea (eastern Mediterranean Sea).
 1199 *Continental Shelf Research*. **13**, 919–939
- 1200 Toti F. (2015) Interglacial vegetation patterns at the Early-Middle Pleistocene transition:
 1201 a point of view from the Montalbano Jonico section (Southern Italy). *Alp. Mediterr.*
 1202 *Quat.* **28**, 2015.
- 1203 Trigo, R. M., Pozo-Vázquez, D., Osborn, T. J., Castro-Díez, Y., Gámiz-Fortis, S., & Esteban-
 1204 Parra, M. J. (2004). North Atlantic Oscillation influence on precipitation, river flow
 1205 and water resources in the Iberian Peninsula. *International Journal of Climatology: A*
 1206 *Journal of the Royal Meteorological Society*, **24**(8), 925-944.
- 1207 Tripathi A. K., Eagle R. A., Thiagarajan N., Gagnon A. C., Bauch H., Halloran P. R. and Eiler J.
 1208 M. (2010) ^{13}C - ^{18}O isotope signatures and “clumped isotope” thermometry in
 1209 foraminifera and coccoliths. *Geochim. Cosmochim. Acta* **74**, 5697–5717. Available at:
 1210 <http://dx.doi.org/10.1016/j.gca.2010.07.006>.
- 1211 Tripathi A. K., Roberts C. D., Eagle R. A. and Li G. (2011) A 20 million year record of
 1212 planktic foraminiferal B/Ca ratios: Systematics and uncertainties in pCO₂
 1213 reconstructions. *Geochim. Cosmochim. Acta* **75**, 2582–2610. Available at:
 1214 <http://dx.doi.org/10.1016/j.gca.2011.01.018>.
- 1215 Turchetto, M., Boldrin, A., Langone, L., Miserocchi, S., Tesi, T. and Foglini, F. (2007)
 1216 Particle transport in the Bari Canyon (southern Adriatic Sea). *Marine Geology* **246**
 1217 (2-4), 231-247.
- 1218 Tzedakis P. C., Channell J. E. T., Hodell D. A., Kleiven H. F. and Skinner L. C. (2012)
 1219 Determining the natural length of the current interglacial. *Nat. Geosci.* **5**, 138–142.
 1220 Available at: <http://dx.doi.org/10.1038/ngeo1358>.
- 1221 de Villiers S., Greaves M. and Elderfield H. (2002) An intensity ratio calibration method

1222 for the accurate determination of Mg/Ca and Sr/Ca of marine carbonates by ICP-
1223 AES. *Geochemistry, Geophys. Geosystems* **3**, n/a-n/a. Available at:
1224 <http://doi.wiley.com/10.1029/2001GC000169>.
1225 Wagner, B., Vogel, H., Francke, A. *et al.* Mediterranean winter rainfall in phase with African
1226 monsoons during the past 1.36 million years. *Nature* **573**, 256–260 (2019)
1227 doi:10.1038/s41586-019-1529-0
1228 Willeit M., Ganopolski A., Calov R. and Brovkin V. (2019) Mid-Pleistocene transition in
1229 glacial cycles explained by declining CO₂ and regolith removal. *Sci. Adv.* **5**,
1230 eaav7337. Available at:
1231 <http://advances.sciencemag.org/lookup/doi/10.1126/sciadv.aav7337>.
1232 Yu J., Elderfield H., Greaves M. and Day J. (2007) Preferential dissolution of benthic
1233 foraminiferal calcite during laboratory reductive cleaning. *Geochemistry, Geophys.*
1234 *Geosystems* **8**.
1235 Zahn R., Pedersen F., Bornhold B. D. and Mix A. C. (1991) Water mass conversion in the
1236 glacial subarctic pacific (54°N, 148°W): physical constraints and the benthic-
1237 planktonic stable isotope record Rainer. *Paleoceanography* **6**, 543–560.
1238

Tables

Table 1: Difference (absolute values in ‰, PDB) of $\delta^{18}\text{O}$ between each species

Samples	MIS	$\Delta^{18}\text{O}$ (‰) <i>C. carinata</i> – <i>U. mediterranea</i>	$\Delta^{18}\text{O}$ (‰) <i>E. crispum</i> – <i>C. carinata</i>	$\Delta^{18}\text{O}$ (‰) <i>E. crispum</i> – <i>U. mediterranea</i>	$\Delta^{18}\text{O}$ (‰) <i>E. crispum</i> – <i>G. ruber</i>	$\Delta^{18}\text{O}$ (‰) <i>U. mediterranea</i> - <i>G. ruber</i>	$\Delta^{18}\text{O}$ (‰) <i>C. carinata</i> – <i>G. ruber</i>
NC-271	19	0.13				2.57	2.44
NC-199	20/19	0.25	0.18	0.43	1.9	2.33	2.08
NC-172	20	0.02				1.64	1.62
DFJ-72	20	0.07				1.49	1.56
DFJ-57	21	0.19				2.30	2.11
DFJ-27/29	22/21	0.00					
DFJ-23	22	0.32				2.67	2.35
DFJ-20	22	0.15				1.83	1.68
IMJ-5b	30	0.24				1.86	1.62
FG-124	31	0.05				2.50	2.45
FG-	31	0.29				1.61	1.32
FG-	31	0.07				3.19	3.13
FG-74	34	0.14				1.50	1.37
FG-39/40	36	0.30					
FG-10/11	36	0.08					

Table 2: $\delta^{18}\text{O}_{\text{VPDB}}$, $\delta^{13}\text{C}_{\text{VPDB}}$, Δ_{47} values and temperatures derived from Δ_{47} values for each sample within each species

Sample	Species	MIS	N	$\delta^{13}\text{C}_{\text{VPDB}}$ (‰)	SE	$\delta^{18}\text{O}_{\text{VPDB}}$ (‰)	SE	Δ_{47}	SE	T- Δ_{47} (°C)	SE
NC-271	<i>C. carinata</i>	19	5	-0.68	0.03	1.96	0.06	0.713	0.007	13.3	2.0
	<i>U. mediterranea</i>	19	8	-0.48	0.02	2.00	0.05	0.705	0.006	15.7	1.6
	Combined	19	13	-0.55	0.02	1.98	0.04	0.708	0.004	14.8	1.3
NC-199	<i>C. carinata</i>	20/19	6	-0.29	0.02	3.57	0.05	0.718	0.006	11.8	1.8
	<i>Elphidium crispum</i>	20/19	27	0.95	0.01	3.53	0.02	0.717	0.003	12.2	0.9
	Combined	20/19	33	0.78	0.01	3.54	0.02	0.717	0.003	12.1	0.8
NC-172	<i>C. carinata</i>	20	4	-0.62	0.01	3.75	0.04	0.736	0.007	7.1	1.8
DFJ-72	<i>C. carinata</i>	20	4	-0.59	0.01	3.50	0.04	0.731	0.007	8.4	1.9
DFJ-57	<i>C. carinata</i>	21	3	-0.59	0.03	2.35	0.06	0.693	0.007	19.2	2.1
	<i>U. mediterranea</i>	21	5	-0.51	0.03	2.33	0.06	0.710	0.007	14.1	2.0
	Combined	21	10	-0.55	0.02	2.34	0.04	0.701	0.005	16.6	1.5
DFJ-27/29	<i>U. mediterranea</i>	22/21	4	-0.43	0.01	2.94	0.04	0.730	0.007	8.6	1.9
DFJ-23	<i>C. carinata</i>	22	4	-0.63	0.01	3.21	0.04	0.727	0.007	9.4	1.9
DFJ-20	<i>C. carinata</i>	22	5	-0.63	0.03	2.94	0.08	0.717	0.009	12.1	2.6
IMJ-5b	<i>U. mediterranea</i>	30	15	-0.44	0.01	3.45	0.02	0.732	0.005	8.0	1.2
FG-124	<i>U. mediterranea</i>	31	11	-0.58	0.01	2.19	0.03	0.711	0.005	13.8	1.5
FG-119/121	<i>U. mediterranea</i>	31	12	-0.43	0.01	2.21	0.03	0.732	0.005	8.1	1.3
FG-103/104	<i>U. mediterranea</i>	31	12	-0.83	0.01	2.75	0.03	0.735	0.005	7.1	1.2
FG-74	<i>U. mediterranea</i>	34	2	-0.52	0.04	3.61	0.09	0.728	0.011	9.2	3.0
FG-39/40	<i>C. carinata</i>	36	4	-0.82	0.03	3.51	0.06	0.716	0.010	12.6	2.9
	<i>U. mediterranea</i>	36	4	-0.71	0.01	3.77	0.04	0.737	0.007	6.7	1.8
	Combined	36	27	-0.72	0.01	3.68	0.03	0.731	0.006	8.4	1.5
FG-10/11	<i>C. carinata</i>	36	4	-0.59	0.03	3.17	0.06	0.712	0.010	13.5	2.9
	<i>U. mediterranea</i>	36	4	-0.57	0.01	3.34	0.04	0.724	0.007	10.3	1.9
	Combined	36	5	-0.57	0.01	3.28	0.03	0.720	0.006	11.2	1.6

* Combined: mix of different benthic species

Table 3: Mg/Ca values and temperatures derived from Mg/Ca values for each samples and species

Samples	MIS	N	Mg/Ca	Species	T-Mg/Ca (°C)	SE	
NC-271	19	1	4.41	<i>G. ruber</i>	25.4	0.8	
NC-199	20/19	1	2.93		20.8	0.8	
NC-172	20	1	5.46		27.8	0.9	
DFJ-72		1	2.94		20.9	0.9	
DFJ-57	21	1	3.59		23.1	0.8	
DFJ-23	22	1	3.35		22.3	0.9	
DFJ-20	20/19	1	2.94		20.9	0.8	
IMJ-5b	30	1	2.41		18.7	0.9	
FG-124		1	4.14		24.7	0.8	
FG-119/121	31	1	3.45		22.7	0.9	
FG-103/104		1	3.51		22.9	0.9	
FG-74	34	1	2.70		19.9	0.8	
NC-271	19	1	1.96		<i>U. mediterranea</i>	12.9	0.8
NC-199	20/19	1	2.09			14.7	1.1
NC-172	20	1	2.09	14.7		1.1	
DFJ-72	22	1	2.04	14.1		1.1	
DFJ-57	21	1	1.89	11.9		0.7	
DFJ-27/29	22/21	1	1.74	9.7		0.9	
DFJ-23	22	1	2.26	17.2		1.2	
DFJ-20	20	1	2.33	18.2		1.3	
IMJ-5b	30	1	1.54	6.9		0.8	
FG-124		1	2.26	17.1		0.9	
FG-119/121	31	1	3.06	28.6		1.7	
FG-119/121		1	2.52	20.9		1.5	
FG-103/104		1	1.94	12.6		1.0	
FG-74	34	1	1.73	9.6		0.7	
FG-39/40	36	1	1.63	8.1	0.8		
FG-10/11		1	1.60	7.8	0.8		

Table 4: $\delta^{18}\text{O}_{\text{SW}}$ records derived from paired $\Delta_{47}\text{-}\delta^{18}\text{O}_{\text{C}}$ in benthic foraminifera, using the O -isotopic fractionation factor at equilibrium of Kim and O'Neil (1997)

Samples	MIS	Species	T- Δ_{47} (°C)	SE	$\delta^{18}\text{O}_{\text{C}}$ (‰)	SE	$\delta^{18}\text{O}_{\text{sw}}$ (‰)	SE
NC-271	19	<i>C. carinata</i>	13.3	2	1.96	0.06	1.6	0.4
NC-271		<i>U. mediterranea</i>	15.7	1.6	2	0.05	2.2	0.4
NC-199	20/19	<i>C. carinata</i>	11.8	1.8	3.57	0.05	2.9	0.4
NC-199		<i>E. crispum</i>	12.2	0.9	3.53	0.02	3.0	0.2
DFJ-72	20	<i>C. carinata</i>	8.4	1.9	3.5	0.04	2.0	0.4
NC-172		<i>C. carinata</i>	7.1	1.8	3.75	0.04	2.1	0.4
DFJ-57	21	<i>C. carinata</i>	19.2	2	2.35	0.06	3.3	0.4
DFJ-57		<i>U. mediterranea</i>	14.1	2.1	2.33	0.06	2.2	0.4
DFJ-27/29	22/21	<i>U. mediterranea</i>	8.6	1.9	2.94	0.04	1.6	0.4
DFJ-20	22	<i>C. carinata</i>	12.1	2.6	3.21	0.04	2.0	0.4
DFJ-23		<i>C. carinata</i>	9.4	1.9	2.94	0.08	2.3	0.6
IMJ-5b	30	<i>U. mediterranea</i>	8.0	1.2	3.45	0.02	1.9	0.3
FG-124		<i>U. mediterranea</i>	13.8	1.5	2.19	0.03	2.0	0.3
FG-119/121	31	<i>U. mediterranea</i>	8.1	1.3	2.21	0.03	0.7	0.3
FG-104		<i>U. mediterranea</i>	7.1	1.2	2.75	0.03	1.0	0.3
FG-74	34	<i>U. mediterranea</i>	9.2	3.0	3.61	0.09	2.4	0.7
FG-39/40	36	<i>C. carinata</i>	12.6	2.9	3.51	0.06	3.0	0.6
		<i>U. mediterranea</i>	6.7	1.8	3.77	0.04	1.9	0.4
FG-10/11	36	<i>C. carinata</i>	13.5	2.9	3.17	0.06	2.9	0.6
		<i>U. mediterranea</i>	10.3	1.9	3.34	0.04	2.3	0.4

Figures and captions

Figure 1: General view of Italy with Montalbano Jonico location (MJS; black star) and Geological context

Figure 2: Lithological and stratigraphical settings of MJ composite for Interval A and B. The composite is from Ciaranfi et al., 2010; the $\delta^{18}\text{O}_{\text{G. bulloides}}$ (planktonic foraminifera) and $\delta^{18}\text{O}_{\text{benthic}}$ (benthic foraminifera) curve are from Brilli, 1998; Brilli et al., 2000 and Ciaranfi et al., 2010. The $^{40}\text{Ar}/^{39}\text{Ar}$ ages of V3-V5 are in Ciaranfi et al., 2010; Maiorano et al., 2010; Petrosino et al., 2015; Simon et al., 2017 and Nomade et al., 2019. The correlation to sapropel stratigraphy was done according to Lourens (2004) and Konijnendijk et al. (2014). Summer insolation is from Laskar et al. (2004). The paleo-water depth was reconstructed in Stefanelli, 2003. G = glacials; IG = interglacials

Figure 3: Temperatures and salinity profiles from the Gulf of Taranto over the first 800 m (data from Pinardi et al., 2016 and World Ocean Atlas 2013); and CO_3^{2-} profile over the first 800 m at the entrance of the Gulf of Taranto (data from Goyet et al., 2000) in red, the closer station from our site location.

Figure 4: Fe-, Mn- and Al/Ca ratio alongside Mg/Ca for all of our benthic sample (*Uvigerina mediterranea*; first column) and planktonic (*G. ruber*; second column). The last box represents Al/Ca versus Mg/Ca for the benthic measurement without the sample DFJ-72, which present a very high value of Al/Ca.

Figure 5: comparison of Δ_{47} - (in square) and Mg/Ca-derived (in triangle) temperatures (2SE), performed on benthic foraminifera (*U. mediterranea*) through Interval A (a.) and Interval B (b.) at MJS, associated to $\delta^{18}\text{O}_{\text{benthic}}$ (Brilli, 1998)

Figure 6: Synthesis of main results for Interval A and B of MJS with $\delta^{18}\text{O}$ curve from benthic foraminifera (Brilli, 1998), our $\Delta\delta^{18}\text{O}$ between benthic and planktonic foraminifera, Δ_{47} -derived subsurface temperatures, Mg/Ca-derived SST, reconstructed subsurface $\delta^{18}\text{O}_{\text{SW}}$ (‰, VSMOW) and the reconstructed paleo-water (Stefanelli, 2003). All uncertainties are at 2SE

Figure 7: $\delta^{18}\text{O}$ curves of benthic and planktonic foraminifera through the Interval A of MJS from 1.25 to 0.9 Ma (Brilli, 1998; Brilli et al., 2000; Ciaranfi et al., 2010) with our subsurface Δ_{47} - and surface Mg/Ca-derived temperatures, the ratio mesothermic vs steppe elements (Joannin et al., 2008), calcareous planktonic foraminifer abundances (red = “warm” species; bleu = “cold” species), *B. begelowii* abundance and plagioclase/quartz ratio (Girone et al., 2013). Grey bands correspond to glacial periods and yellow band to the climatic optimum of MIS 31

Figure 8: Zoom on MIS 20-19 from 0.805 to 0.755 Ma, with our Δ_{47} -derived subsurface temperatures compared to high-resolution of benthic $\delta^{18}\text{O}$ and $\delta^{13}\text{C}$ curves (performed on *M. barleanum* and *C. carinata*; Nomade et al., 2019); principal component of SST from calcareous nannofossils and foraminifera (Pc1; Maiorano et al., 2016); percentage of *N. pachyderma* left coiling (Maiorano et al., 2016), ratio mesothermic vs steppe elements (Bertini et al., 2015) and summer insolation at 65 °N from Laskar et al. (2004)

Figure1

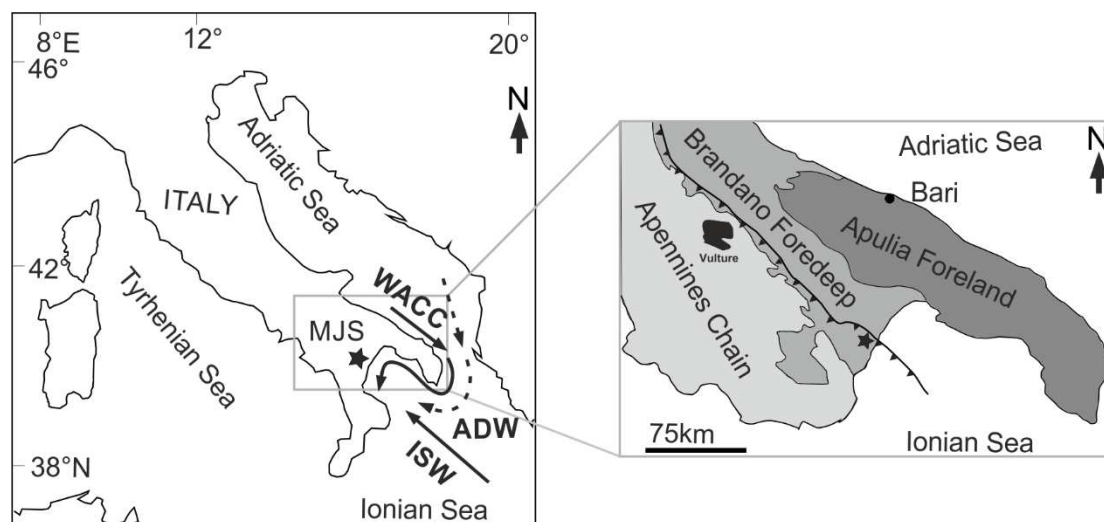


Figure 2

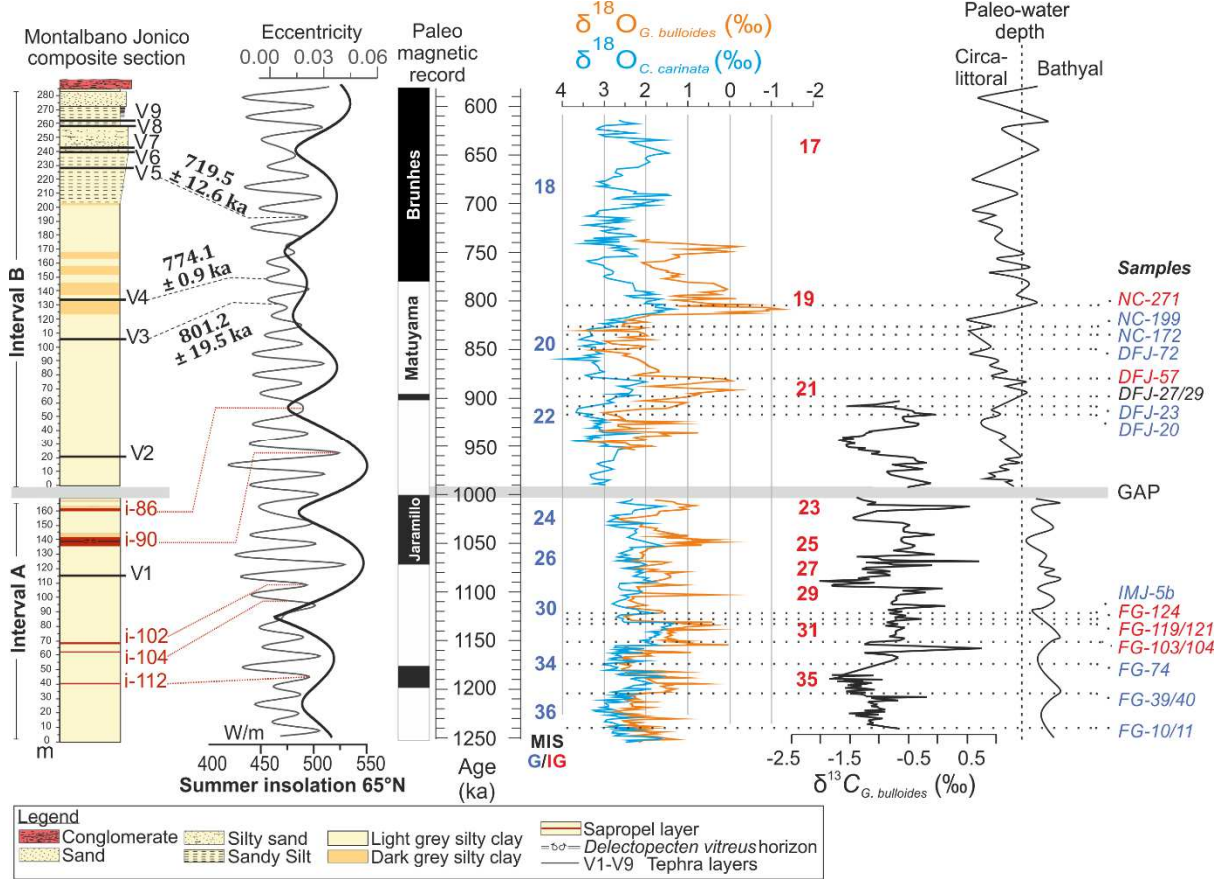


Figure 3

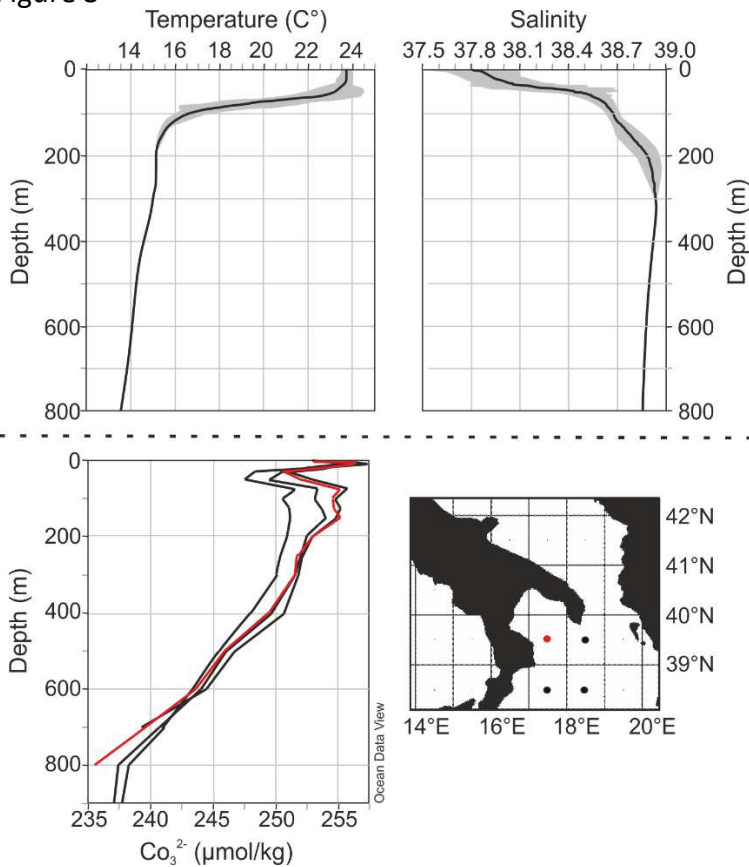


Figure 4

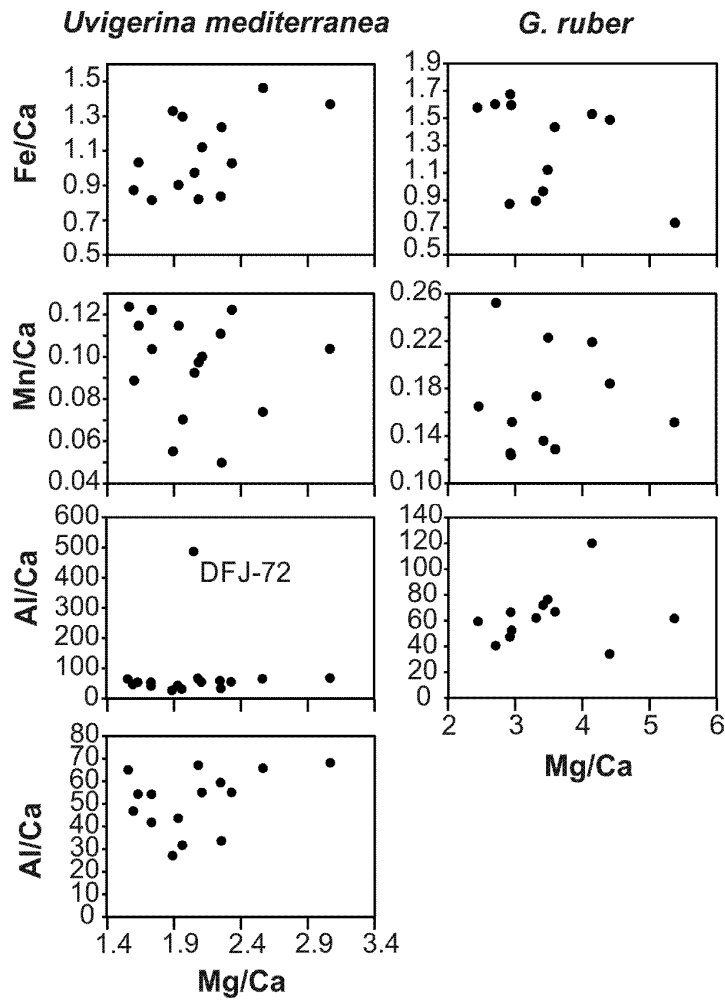


Figure 5

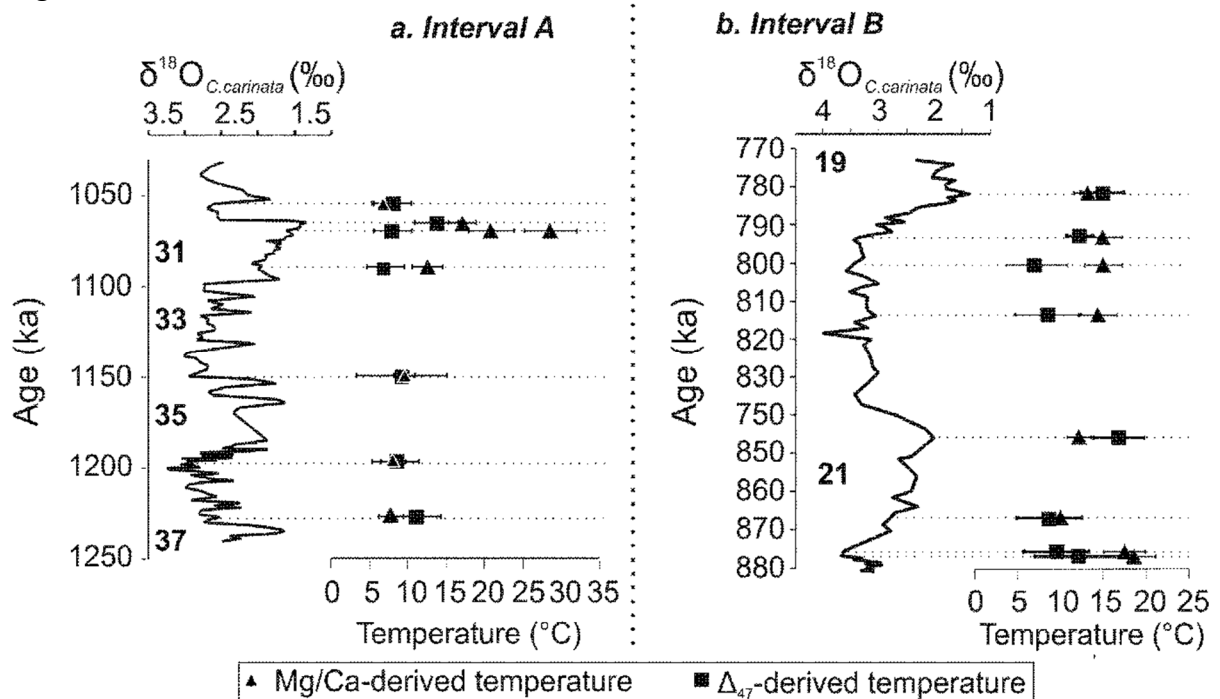


Figure 6

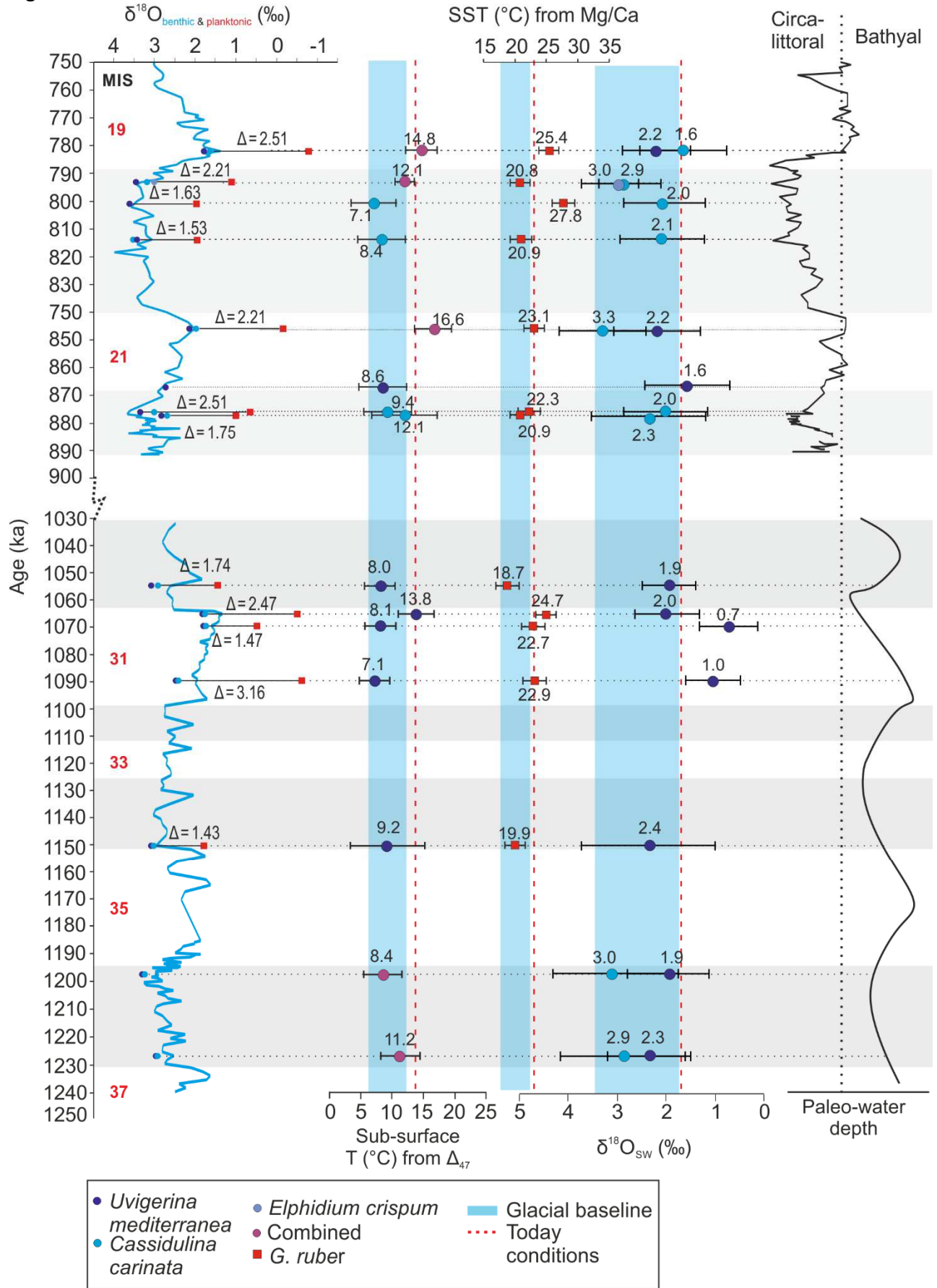


Figure 7

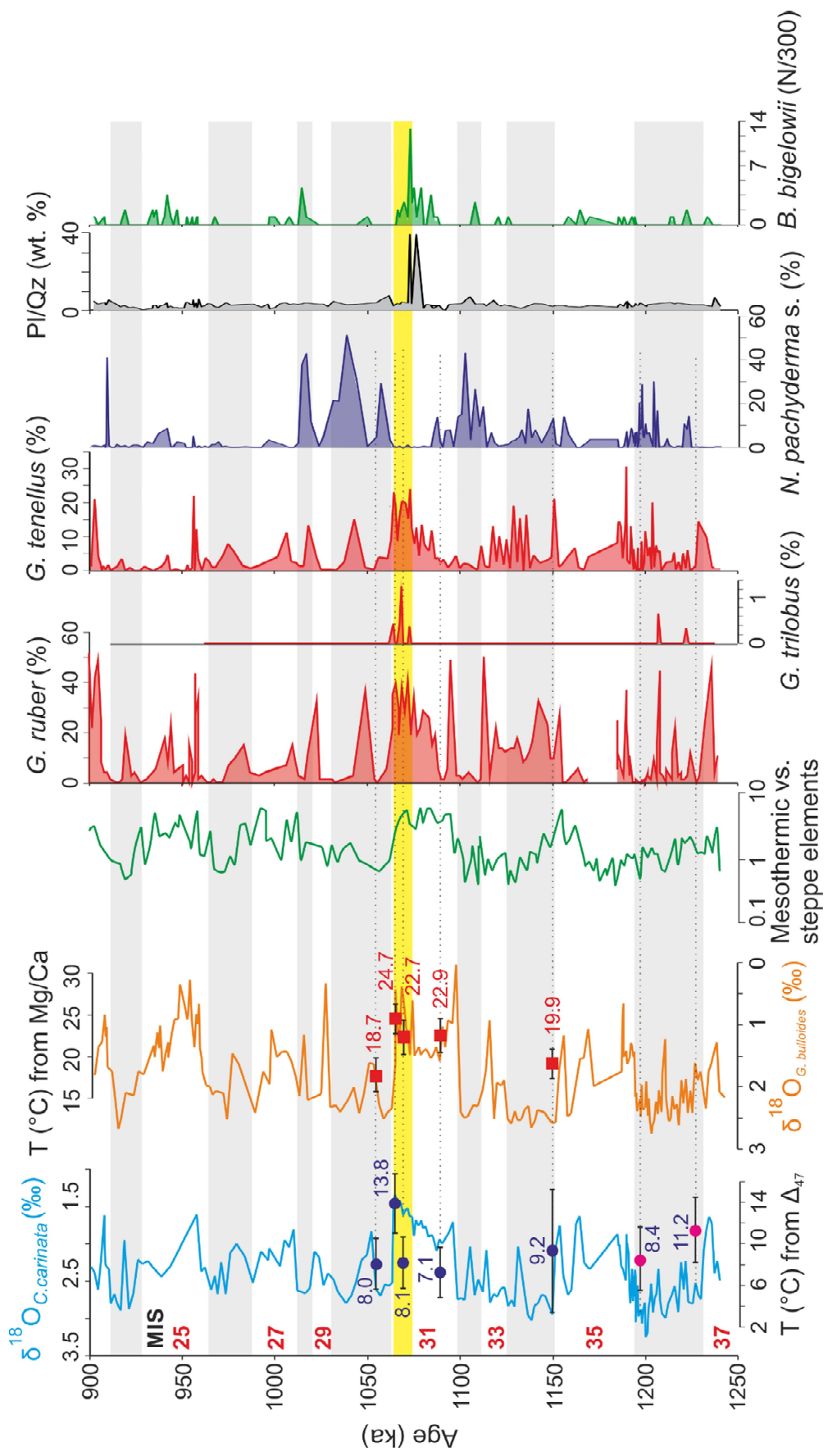


Figure 8

